Influence of the self-excited induction generator in the improvement of the energy efficiency in isolated PAT systems

João Francisco Cabrita Caeiro

Thesis to obtain the Master of Science Degree in

Electrical and Computer Engineering

Supervisors: Prof. Paulo José da Costa Branco
Prof. Modesto Sanchez Pérez

Júri

Chairperson: Prof. Célia Maria Santos Cardoso de Jesus
Supervisor: Prof. Paulo José da Costa Branco
Members of the Committee: Prof. Helena Margarida Machado da Silva Ramos

June 2019

Declaration

I declare that this document is an original work of my own authorship and that it fulfills all the requirements of the Code of Conduct and Good Practices of the Universidade de Lisboa.

Abstract

The substitution of the pressure reducing valves (PRV) with Pump working as a Turbine (PAT) have been considered in the past years for being a viable solution as it provides both pressure control and energy savings, at a low price.

The using of PAT was identified by many researchers to improve the energy efficiency in the water systems. However, most of the researchers consider the hydraulic machine connected to the electrical grid, which may be inconvenient when these recovery systems are located in rural or remote areas. To improve the knowledge of the efficiency in these recovery systems for rural areas, this thesis contributes for a further study and optimization of the off-grid PAT systems with induction generators (IG). This thesis proposes a methodology to obtain the best optimization for the excitation capacitor valuer of PAT-SEIG (Self-excited Induction Generator) system while operating under different speeds and loads. This has the goal of maximize the global energy efficiency of the system which it is vital in off-grid systems.

Here, it can be found a proper solution considering the variation of the electrical parameters of the IG according to its magnetizing level. These results showed increase accuracy for modeling the SEIG as an analytical model and simulation model.

The accuracy of the analytical model improved, reducing the error between analytical and experimental results. It means that it is possible to simulate all the SEIG+PAT system in the lab and its behavior with different stimuli.

Keywords: Energy efficiency, Self- Excited Induction Generator (SEIG), Pump working as a Turbine (PAT)

Resumo

A substituição de válvulas redutoras de pressão (VRP) com bombas como turbina (PAT) tem sido, nos últimos anos, objeto de estudo para a determinação de uma solução viável para o controlo da pressão e capacidade de recuperar energia, a um preço baixo.

O uso das turbinas foi considerando por vários autores como uma forma de aumentar a eficiência energética nos sistemas de água. Porém, a maior parte das pesquisas considera apenas a ligação da turbina hidráulica a uma rede elétrica, o que para o caso de estudo, zonas rurais e de remoto acesso, não é uma opção viável. Este trabalho contribui para um aprofundamento no estudo e otimização das turbinas operando como bombas de pressão com geradores de indução (IG), para o desenvolvimento da eficácia dos sistemas de recuperação de energia nos locais mencionados. Esta tese propõe uma metodologia do sistema PAT+SEIG que opera com diferentes cargas e diferentes velocidades de rotação. Considerando a variação dos parâmetros elétricos nas condições de isolamento da rede e uma escolha adequada de condensadores, necessário para manter a máquina a rodar nos parâmetros nominais, pode-se encontrar aqui uma solução válida para maximizar o sistema de recuperação de energia. É dada uma atenção especial ao possível impacto dos parâmetros do SEIG na otimização do sistema de recuperação. Neste trabalho foi também possível encontrar modelos de análise e de simulação do SEIG, que são mais precisos comparando com trabalhos anteriores, dado a introdução dos parâmetros de magnetização nos modelos.

Palavras-chave: Eficiência energética; Bomba como Turbina; Gerador de Indução Autoexcitado (SEIG);

Acknowledgements

The accomplishment of this work would not have been possible without the help of several people. Firstly, I would like to thank my supervisors, Prof. Paulo José da Costa Branco and Professor Modesto Pérez Sánchez, for their guidance and encouragement. I would also like to thank Professor João Fernandes, for his help and guidance through this project. In addition, I would like to thank to my family for the constant support and motivation as well as my girlfriend, for her constant belief in me whenever I had a fall-back and lack of motivation. Without her I would have probably not been able to finish this thesis. I also want to thank to the REDAWN project, that enabled me to make this experimental thesis. Finally, I want to thank my group of colleagues and friends, for the companionship and motivation during the time I was doing this thesis.

Table of Contents

Índice

Lists

List of Figures

List of Tables

List of Acronyms

AC	Alternating Current
DC	Direct Current
IG	Induction Generator
PAT	Pump running as Turbine / Pump as Turbine
PRV	Pressure Reducing Valve
SEIG	Self-Excited Induction Generator
SG	Synchronous Generator
SOC	State of Charge
WDN	Water Distribution Network
WDS	Water Distribution System
WTS	Water Transmission System

List of Symbols

A	*Amp*
a	Stator frequency in values *per unit*
b	Rotational speed in values *per unit*
C	Capacitance value of the excitation system of the SEIG
f	Induction generator actual stator frequency [Hz]
f_s	Grid frequency [Hz]
F	*Farad*
g	Gravitational acceleration [m/s^2]
Hz	*Hertz*
I_0	Phase current for no load condition
I_a	DC motor armature current
I_{cc}	Phase current for short-circuit / blocked rotor case
I_f	DC motor field current
I_m	Magnetizing current
I_r'	Rotor current
I_s	Stator phase current
L_L	Load inductance
L_m	Magnetizing inductance
L_r	Rotor inductance
L_s	Stator inductance
N	Rotational speed of the induction machine [rpm]
N_1	Number of stator windings

N_2	Number of rotor windings
N_s	Synchronous frequency [rpm]
p	Number of pole pairs of the induction machine
P_0	No load active power
P_{cc}	Short-circuit active power
P_{IN}	Total power at the entrance of the DC motor
P_{loss}	DC motor total losses
P_{mec}	Mechanical power
P_{OUT}	DC motor mechanical output power
P_{rot_loss}	DC motor rotational losses
P_s	Active power of the induction machine
$pf \equiv \cos\varphi$	Power factor
Q_0	No load reactive power
Q_{cc}	Short-circuit / blocked rotor reactive power
Q_s	Induction machine stator reactive power
R_L	Load resistance
R_m	Induction machine magnetizing resistance, represents the core losses
$R_r{}'$	Induction machine rotor resistance
R_s	Induction machine stator resistance
s	Slip
S_0	No load apparent power of the induction machine
S_{cc}	Short-circuit apparent power of the induction machine
U_a	DC motor armature voltage

U_f	DC motor field voltage
V	*Volt*
V_0	Induction machine no load phase voltage
V_{cc}	Induction machine short-circuit phase voltage
X_c	Capacitor Reactance
X_L	Load inductive reactance
$X_r^{'}$	Induction machine rotor reactance
X_s	Induction machine stator leakage reactance
Y_C	Admittance of the bank of capacitors
Y_{in}	Induction machine equivalent admittance
Y_L	Load admittance
Y_r	Equivalent admittance of rotor and magnetizing branch
Y_s	Stator equivalent admittance
Y_t	Total equivalent admittance of the SEIG
ω	Angular frequency of the machine [rad/s]
ω_r	Rotational speed of the rotor [rad/s]
ω_s	Synchronous frequency [rad/s]
φ	Magnetic flux [V/Hz]
$\emptyset_{leakage}$	Magnetic flux leakage [V/Hz]
$\emptyset_{linkage}$	Magnetic Flux Linkage [V/Hz]

1. Introduction

The need to find new and more efficient ways to produce energy without the use of fossil fuels has been one of the most important aspects of engineer for the last 20 to 30 years. In this context, investment was made in different renewable energy sources with small environmental impact, including hydroelectric power generation. Although the hydroelectric power generation has been one of the renewable energy sources that have suffered fewer advances in the last decade, there has been a renewing interest in this technology, especially in the small and micro-scale hydropower sources (Capelo et al., 2017). The goal of this study is important for cases where the generation of energy supplies low consumptions.

Regarding water management in different supply systems, the sustainability has been improved by reducing leakages as well as by applying pressure-control tools to the system. This has been provided throughout the years with pressure reducing valves (PRV's), which are still being optimized to reduce the pressure and hence to reduce the leakage (Wright, Abraham, Parpas, & Stoianov, 2015). However, the problem is that these PRV's do not produce energy and the water that pass through them cannot be recovered as a form of electrical energy. That is where the Pump working as a turbine (PAT) enters in the picture because it does a similar job as a PRV (Buono, Frosina, Mazzone, & Cesaro, 2015), however it can recover some energy. In some contexts, such as rural and remote areas and big farms, the use of the PAT can be a reliable source of energy and it represents a high reduction in the implementation cost. According to Ramos & Borga (2000) it is said "*for a pump operating under maximum output power, the relative efficiency is up to 80%*". Although it may not be as efficient as a hydro-turbine, the relation of cost/benefits is higher in the PAT case, because it is cheaper, easier to build and has a satisfying durability. The use of PAT is also considered a good and economic approach, in locations where the water supply is relatively constant.

Although there has been, in the last 20 years, a greater interest in the study of off-grid cases while working a PAT, the implication of the electrical parameters in the induction generator efficiency of the system has seldom been tackled in past researches. The focus is still the hydraulic recovery of power, such as in Fribourg where the recovered energy represents 10% of the available energy in water supply systems (Samora, Franca, Schleiss, & Ramos, 2016). However, there was not any consideration on the influence of the electrical machine in the efficiency of the recovered energy or any consideration of electrical parameter variation of the generator as a factor of recovering energy.

The research developed during the master thesis proposes a methodology to obtain the best efficiency of the PAT-SEIG system when operating under different speeds and loads. The use of this methodology will allow water managers to know the best rotational speed of the machine in order to maximize the energy recovered considering the variable load in the circuit. This methodology was applied in a laboratorial prototype, where the electrical experiment, numerical and simulation analysis

were developed and compared to previous researches in this same area (Fernandes et al., 2018), reaching interesting results and conclusions to improve the energy efficiency in the recovery water systems.

The objective of this thesis can be divided into the following topics:

- Complete study from the induction machine;
- Proposes a methodology to obtain the best efficiency of the SEIG (Self-Excited Induction Generator) system when operating under different speeds and loads
- Verification of the impact of the SEIG electrical parameters in the efficiency of the PAT system;
- Selection of capacitors for the SEIG is essential to maximize the energy efficiency;
- Comparison between analytical models, with and without the iron losses, and the impact of choosing the wrong capacitor values, in the influence of the variation of each induction generator (IG) electrical parameter in the capacitor value and in the final system efficiency.

This thesis is divided into five chapters, which include the following components:

- In Chapter 1 is provided an introduction and overview of the work;
- In Chapter 2 is performed a brief review of the state of the art related to the use of the SEIG system in different energy areas;
- In Chapter 3 is performed a study on the induction machine and how it would behave as well as its electrical parameters when under non-normal conditions.
- In Chapter 4, a complete study of the Isolated Induction Generator, named the Self-Excited Induction Generator (SEIG), with simulation and experimental work;
- In Chapter 5, some general conclusions of the performed work are given and some comments on the future work.

2. State of Art: Off-Grid SEIG overview

In this chapter there is going to be made a brief overview of what has been investigated on the latter years on off grid self-excited induction generators (SEIG). There will be given explanation on how this system work and how the SEIG works under steady state and transient operations.

2.1 Self Excited Induction Generator: Characteristic

With the increasing trend toward the use of renewable energy sources for electricity generation such as the following: micro-hydro, wind energy, biogas and solar energy, a greater emphasis is being laid on the development of a low-cost, least maintenance, simple and robust generator unit for standalone isolated applications (Singh, Singh, & Tandon, 2010). Since small hydro and wind energy sources are available in plenty, the utilization of the SEIG promises to accomplish the future energy needs.

Traditionally, over the last few decades the synchronous generator (SG) has been a more common approach for power generation but it has been sturdily been substituted for induction generators due to its features that has a bigger interest over the conventional SG (Raina & Malik, 1983).

Self-excited induction generators have been a subject of considerable research due to its potential and simplicity as a device that converts motion into producing electricity in off-grid, standalone mode using different types of prime movers. SEIG even has the capacity of adaptability which means that this generator can be used for all different renewable energy systems due to its simple perception of converting mechanical into electrical energy.

The major drawback of a SEIG is the poor regulation of its frequency and voltage under prime mover speed and load perturbations which, without the proper use of some power electronics and some feedback controllers, there is no possibility of giving a steady and continuous supply that can feed a load. The generated terminal voltage and the output frequency depend on the excitation capacitance, the three-phase induction machine parameters, the electrical passive load and the prime mover speed (Kumawat, Chourasiya, Agrawal, & Paliwalia, 2015)
On basis of rotor construction, induction generators are characterized as: wound rotor and squirrel cage. This basic rotor characterization is better explained in the introduction of the chapter 3. Depending upon the prime movers used (constant speed or variable speed) and their locations, generating electrical schemes of the SEIG can be classified as (Kumawat et al., 2015; Raina & Malik, 1983):

- Variable-Speed Constant-Frequency (VSCF);
- Variable-Speed Variable-Frequency (VSVF);
- Constant-Speed Constant-Frequency (CSCF);

For this system purpose the Constant-Speed and Constant-Frequency generator is useful since with no-grid operation there is no possibility of maintaining either constant frequency or speed.

A VSCF generator is a generator where the frequency must be controlled by the grid or a bus frequency control and the speed remain variable. This type of generator is very common among wind driven systems. It is necessary a speed controller to obtain maximum power from the wind and a converter to change variable frequency of the generator to constant frequency of output voltage.

The most common use of a Variable Speed Constant Frequency generator is the doubly fed induction generator (DFIG). According to Pena, Asher, Clare, & Cardenas (1996), DFIG is able to generate power from both stator and the rotor. This characteristic can only be exploited if bidirectional power flow capability for the rotor excitation is provided.

The generator is doubly fed as follows: not only the stator is supplied by the DC machine represented in Figure 2-1, with voltage at synchronous frequency, but is also fed by the AC-DC-AC line. The AC-DC-AC line is represented by two converters and a DC link. At the rotor's side, the voltage applied by the frequency converter has such a frequency that if imposed on the rotor speed a synchronous rotating field appears.

The frequency that comes from the DC machine goes to an AC/DC converter, the front-end converter in Figure 2-1. Subsequently it is converted through a DC link, where it is eliminated its DC frequency component. Finally, it is re-converted to AC frequency by an DC/AC rotor side inverter, with the desired output frequency for the generator.

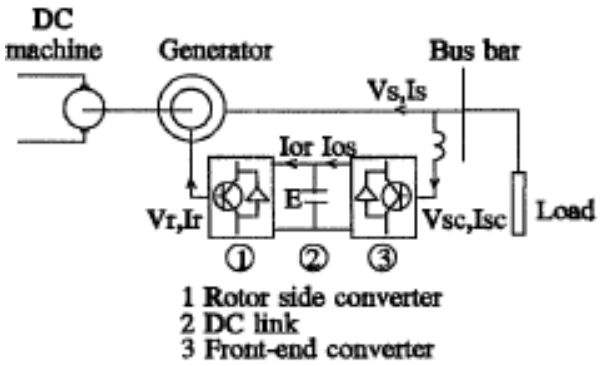

Figure 2-1 - Standalone wound rotor generator scheme adapted from Pena et al. (1996)

The frequency converter controls the voltage amplitude and frequency that goes through the generator. It is also able to provide current in the stator, due to the creation of the synchronous rotating field. Those frequency converters and inverters work by imposing rotor current with slip frequency, which then supply the isolated load.

This system needs to be linked with an infinite bus or a source that supplies a constant frequency/voltage into the system, in order to impose the frequency. So, this system is harder to apply in very isolated areas because there is a need for a support system such as a grid or a generator, that supplies constant voltage and frequency, for variable speeds.

For variable speed operation the DFIG must supply constant voltage and frequency to the isolated load. If the voltage drop in the stator resistance is negligible, the stator voltage can be regulated indirectly by controlling the stator flux.

The next equations describe the DFIG in a synchronous rotating d-q reference frame:

$$\emptyset_{d_s} = L_s.i_{d_s} + L_m.i_{d_r} = L_m.i_m \quad (2.1)$$

$$\emptyset_{q_s} = L_s.i_{q_s} + L_m.i_{q_r} = 0 \quad (2.2)$$

$$\emptyset_{d_r} = L_m.i_{d_s} + L_r.i_{q_r} \quad (2.3)$$

$$\emptyset_{q_r} = L_m.i_{q_s} + L_r.i_{q_r} \quad (2.4)$$

$$V_{d_s} = R_s.i_{d_s} + \frac{d\emptyset_{d_s}}{dt} \quad (2.5)$$

$$V_{q_s} = R_s.i_{q_s} + \frac{d\emptyset_{q_s}}{dt} \quad (2.6)$$

$$V_{d_r} = R_r.i_{d_r} + \frac{d\emptyset_{d_r}}{dt} - w_{slip}.\emptyset_{q_r} \quad (2.7)$$

$$V_{d_r} = R_r.i_{q_r} + \frac{d\emptyset_{q_r}}{dt} - w_{slip}.\emptyset_{d_r} \quad (2.8)$$

$$w_{slip} = w_e - w_r \quad (2.9)$$

$$\theta_{slip} = \theta_e - \theta_r \quad (2.10)$$

$\emptyset_{d_s}$, $\emptyset_{q_s}$, $\emptyset_{d_r}$, $\emptyset_{q_r}$, V_{d_s}, V_{q_s}, V_{d_r}, V_{d_r}, i_{d_s}, i_{d_r}, i_{q_s}, i_{q_r} are the stator and rotor fluxes, voltages and current in this order and w_{slip} is the slip frequency. L_s , L_m , L_r are the stator, magnetizing and rotor inductances respectively. R_s and R_r are the stator and rotor resistances respectively. The two currents i_{d_r} and i_{q_r} are imposed in the rotor using a voltage fed current regulated converter. Constant stator frequency is achieved by applying rotor currents with a frequency equal to the slip frequency. θ_e is the electrical stator flux position and it is obtained by integrating the stator electrical frequency.

A variable-speed variable-frequency (VSVF) is normally used for systems where the generator gives a higher rated power to a load without an excessive overheating of the machine. In this case, the purpose of constant and rated frequency and speed is irrelevant. This idea is gaining importance for stand-alone wind and hydropower applications. Normally, this type of generator is set as a Double Output Induction Generator (DOIG) (Giraud & Salameh, 1998). Figure 2-2 shows an application of a Variable-Speed Variable-Frequency Double Output Induction Generator, where it is visible a stator and rotor power feed to a load.

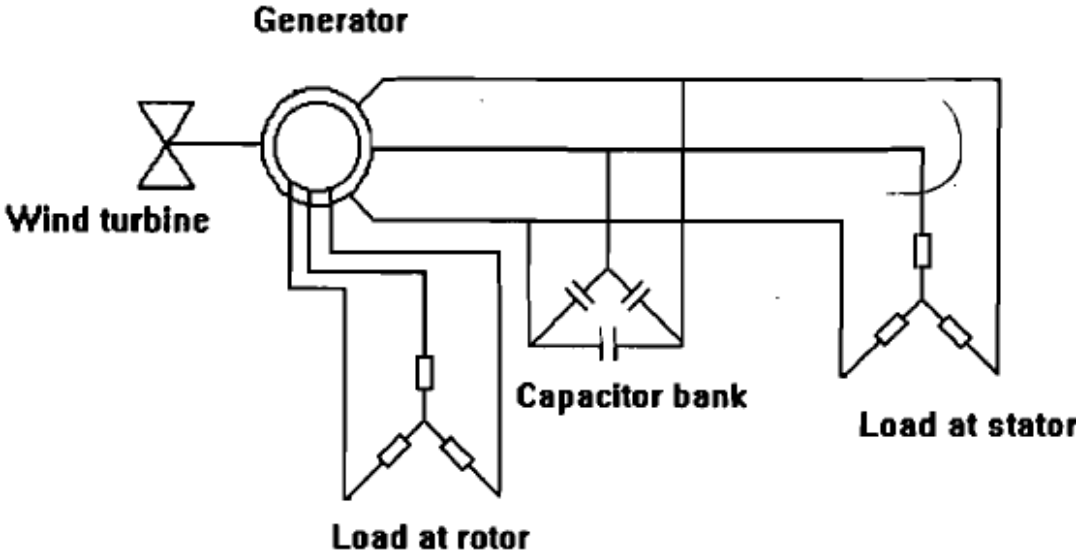

Figure 2-2 - Diagram of a VSVF induction generator on a Wind Turbine Application (Giraud & Salameh, 1998)

This system usually employs a squirrel cage induction generator to feed frequency insensitive loads. If an appropriate capacitor bank is connected across the terminals of an externally driven induction machine, a voltage is built-up by the residual magnetism in the rotor circuit. In this system, a steady and stable operation voltage results when the capacitors are able, for each frequency and speed, to provide adequate reactive power to induce a current from the rotor to the stator. Thus, the generator can supply power, from both the stator and the rotor, to supply load needs. If the capacitor bank is not well dimensioned for this VSVF generator, it can not excite properly the whole system

This operating point, due to many degrees of freedom, it is highly complex and through the last years, there has been some research in the area of power electronics to somehow control the variance of both speed and frequency (Xu, Xie, Wang, & Shi, 2017).

Figure 2-3 shows the scheme of the equivalent circuit of the SEIG, including the generator load, the capacitive load and the resistive load.

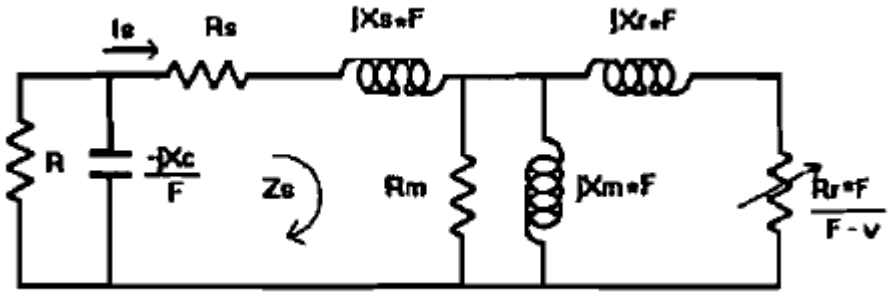

Figure 2-3 - Per-phase equivalent circuit of generator, capacitor load, stator load and variable rotor load (Giraud & Salameh, 1998)

In this figure it is possible to see three different areas that represent the SEIG system: the generator, the capacitor and the induction machine. All the system parameters and variables in this circuit are defined as per-phase and per-unit values based on the rated values of the induction machine:

R_s: per-unit resistance of the stator;
R_r: per-unit resistance of the rotor (referred to the stator);
R_m: per-unit resistance representing the core losses;
R: resistive load on the stator;
X_m: per-unit magnetizing inductance;
X_s: per-unit stator leakage inductance;
X_r: per-unit rotor leakage inductance
X_C: reactive capacitance;
F: per-unit stator frequency
v: per-unit rotor speed

3. Induction Machine

An Induction Machine is an alternating current machine. It operates by supplying the stator directly with a tri-phase alternating current, which induces a magnetomotive force in the rotor that eventually will make it spin. It has the same physical stator as a synchronous machine with a different rotor construction, and it does not need an additional DC field current. However, its rotor rotational speed is always lower than the rotational stator speed, called synchronous speed (as a motor), and this variation is named slip.

There are two types of three-phase induction machines: wound and squirrel-cage rotor (Figure 3-1). A wound rotor is composed by a three-phase winding, which can be accessed by a set of carbon brushes. A squirrel-cage rotor is composed by conducting bars embedded in slots in the rotor, short-circuited at each end by conducting end rings. In these conditions the rotor currents are induced not only due to the flux linkage between the rotor and stator circuits but also due to the flux density distribution in the rotor.

Due to its simplicity, robustness and the fact that is a cheap option it is less costly, the squirrel-cage design presents high advantages, and so it is the most commonly used. For motor type operation, induction machines are by far the most common type used in industrial and commercial applications. Although its use as a generator is seldom used thanks to its unsatisfactory performance characteristics, in wind and hydraulic applications the induction machine is commonly used as a generator.

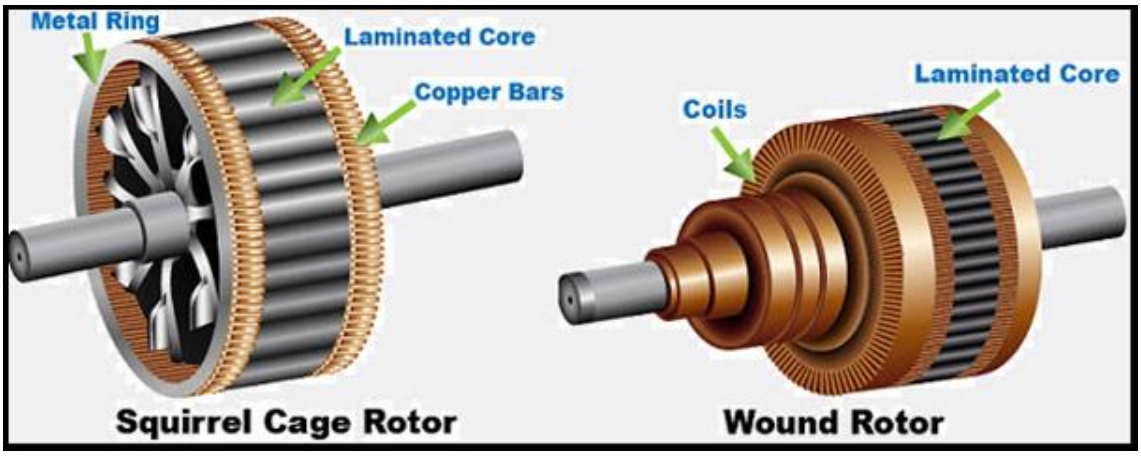

Figure 3-1. Illustrative image of both types of induction machines

The equivalent circuit of a squirrel cage induction machine is expressed in Figure 3-2. The circuit represents one phase of the machine.

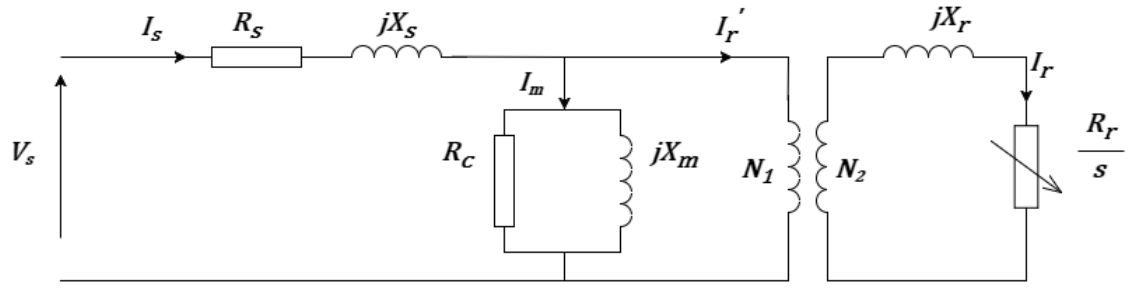

Figure 3-2. Equivalent of one phase Induction Machine (Eltamaly, 2002)

The electrical equivalent circuit from Figure 3-2 can be divided into three different parts: stator, magnetization and rotor. The resistance R_S represents the resistance of the stator winding and X_S represents the stator leakage reactance. The resistance R_C represents the core losses and X_m represents the magnetization reactance. For the air gap, N1 and N2 represent an ideal transformer between stator and rotor windings. Finally, for the rotor side, X_r and $\frac{R_r}{s}$ represent the rotor's reactance and resistance, respectively.

Below, in Figure 3-3, it can be seen a simplified model, in which the air gap (ideal transformer) area is neglected, and so the rotor values are now referred to the primary (stator).

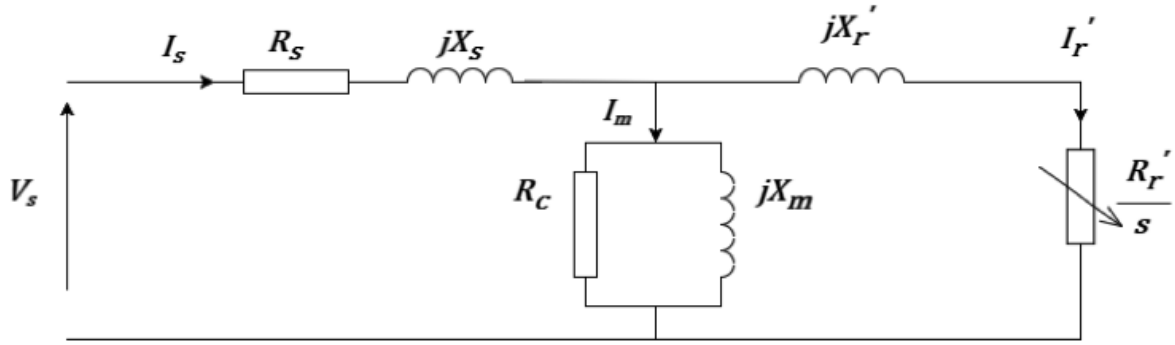

Figure 3-3. Simplified equivalent of an induction machine, adapted from Eltamaly (2002)

For an induction generator isolated from the grid a constant reactive power source is needed to feed it and make it able to work. Hence it is required an external reactive power source.

From here, an analysis of the Induction Generator isolated from the grid is necessary. This type of IG application is named the Self-Excited Induction Generator (SEIG).

In this chapter it is only analyzed the induction machine while the SEIG is going to be analyzed in higher detail in further chapters. In this chapter the parameters of the induction machine and their variations with frequency and voltage will be studied.

In order to understand the off-grid scenario it is necessary to place the induction machine where the frequency and voltage are not stable, and thus complete one of the goals of this thesis, that is the off-

grid conditions performed on a induction generator. So, in this chapter, with the aid of an experiment where both induced voltage and frequency were not regulated it will be possible to determine how the parameters and which parameter is more sensible to frequency and voltage variations. Finally, one of the main questions to be answered is: which and how parameters change most considerably in order to find the best reactive power to maximize the SEIG.

In Figure 3-4 it is showed the induction machine used for the experiments that will allow to answer the question stated above, following the nameplate data of the induction machine in Table 3-1:

Figure 3-4. Induction machine used for experimental tests.

Table 3-1. Nameplate data of the induction machine

3 – phase induction machine	
Frequency	50 Hz
Voltage	400V
Current	1.6A
Output Power	0,55 KW
Power Factor	0.73
Speed	910 rpm

3.1. Induction Machine – Electrical Parameters

As it can be seen from Figure 3-5, the induction machine is characterized by a set of parameters. They are all going to be tested if there is a significance variation in its value with change in frequency and voltage. To create these testing conditions, the machine should be tested in two different conditions, no load and blocked rotor test.

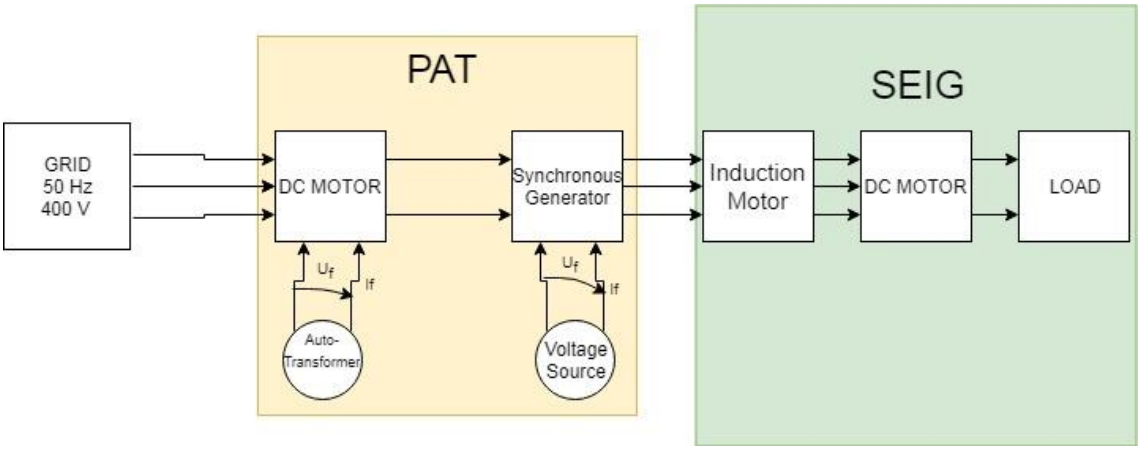

Figure 3-5. Chart explaining the experiments which replicate the behavior of a SEIG

Figure 3-5 conceptually illustrates the experiment made and presented in this chapter. It is divided in three major areas: the grid, the PAT and the SEIG. The experimental conditions to operate this set of components were the following:

- The grid will be represented as a normal tri phase grid which provides the system with a voltage of 400V and a frequency of 50Hz. The PAT area is where the pump working as a turbine is simulated and in there it is imposed the frequency and the voltage that is channeled to the SEIG.
- The PAT is simulated through two machines, a DC motor and a synchronous, with two different purposes. The DC motor is the machine which all the machines depends on its speed. It is the machine that dictates the frequency and speed of the remaining machines. It is controlled through an Autotransformer, which receives the grid voltage and frequency and regulates the frequency of the remaining system. The synchronous generator is responsible for regulating the voltage that runs to the SEIG system. With the help of the voltage source it is possible to control the field voltage that directly affects the voltage of the SEIG.
- In this system, two machines and a load characterize the SEIG. First, the frequency and voltage go through the induction machine where it is possible to obtain the values for voltage, current, active and reactive power, the power factor, rotational speed and frequency. The DC motor is essential to link the induction machine to the load due to the fact that the induction machine used in the experiment was a tri-phase machine and the load is a one-phase resistor so it is necessary to make the transition. We can consider also the DC motor as load. Its main role was to work as a prime mover, in order to help analyze the behavior of the induction generator in study.

For this chapter, the load is not required because in the blocked rotor test and no-load test it is irrelevant. The machine in these conditions simply is unable to supply any kind of load.

Before starting the tests, with the help of a digital multimeter, connected between two phases of the machine, it was possible to estimate the stator resistance value. If it is assumed that the machine has a tri-phase balanced system, which is demonstrated on the experimental results, it is only needed to divide by two the resistance that is shown in the multimeter to estimate the stator resistance in a phase ($R_e = 2R_S = 36{,}6\Omega = 18.8\Omega$)

For the tests executed in this section, a small set of materials was used: an auto transformer, a digital multimeter FLUKE, a digital tachometer (to measure the machine rotational speed), a voltage source and a digital multimeter fluke with the responsibility of measuring the frequency of each test.

3.1.1. Blocked Rotor Test

In this experiment the motion of the rotor is blocked, which is necessary to determine the parameters in the two main branches of the induction machine, the primary and secondary. The objective was to increase the phase current until the field current of the SG, I_f, reaches its nominal value of 1.6A. For each frequency was set 8 points with different field current, I_f, of the SG. These field current values vary between an interval of: $I_f(20hz{:}\,60Hz)$: $\alpha\,[0.7; 1.6][A]$.

The induction machine's equivalent circuit, in this case can be simplified as shows Figure 3-6, where the magnetization branch of the circuit is neglected. This approximation is reasonable considering that the core losses R_m are much higher than the rotor losses R_r. This statement is verified with the no-load and blocked rotor test. It is also stated that the slip is considered $s = 1$, due to speed being $N = 0\,rpm$.

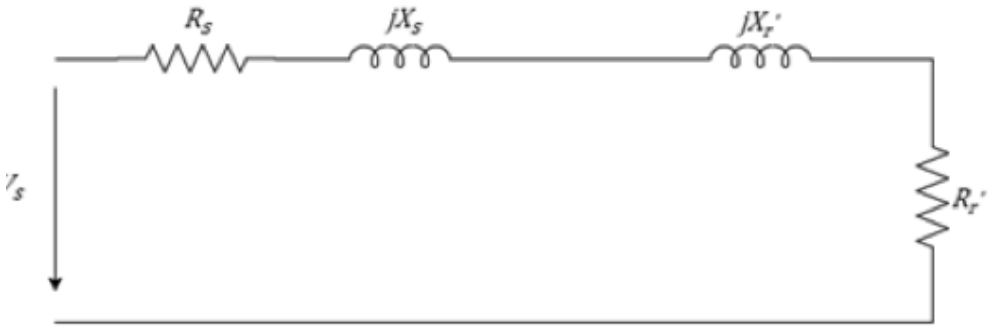

Figure 3-6. Equivalent circuit of an induction machine for blocked rotor case, adapted from Paiva (2011)

In order to obtain the stator and rotor inductances (X_s and X_r') as well as the rotor resistance (R_r') the equivalent electrical system must be studied. In order to do that we have to use the equations (3.1) – (3.3) are used.

$$Q_{sc} = S_{sc} * \sin\varphi \tag{3.1}$$

$$R = R_s + R_r' = \frac{P_{sc}}{I_{sc}^2} <=> \frac{P_{sc}}{I_{sc}^2} - R_s = R_r' \tag{3.2}$$

$$X = X_s + X_r{}' = \frac{Q_{sc}}{I_{sc}{}^2} \tag{3.3}$$

Due to the design of the circuit and the values of current and voltage are taken it is considered the short circuit current and voltage are equal to the stator voltage. Table 3-2 shows the measurements taken from this experiment, at 20 Hz frequency. The values on the first line are the 8 points in which the field current of the synchronous generator was varied until reaching its nominal value. The tachometer has measured no rotation in the motor as expected due to the rotor being blocked from rotating.

The remaining frequencies are displayed in the Annex C.

Table 3-2. Test results for 20 Hz frequency

I [A]	0.64	0.7	0.85	1	1.15	1.3	1.45	1.6
U1 [V]	21.3	25.8	29.2	35.3	40.2	43.6	47.8	52
U2 [V]	21.1	25.5	29.1	35.1	40.6	43.9	48.1	51.7
U3 [V]	21.3	25.6	29.1	35.2	40.5	43.9	43.6	51.5
I1 [A]	0.64	0.74	0.85	1.02	1.18	1.28	1.42	1.58
I2 [A]	0.64	0.74	0.84	1.02	1.18	1.29	1.42	1.57
I3 [A]	0.66	0.76	0.86	10.2	1.19	1.29	1.43	1.58
P1 [W]	0.012	0.017	0.022	0.032	0.042	0.05	0.061	0.073
P2 [W]	0.012	0.017	0.021	0.031	0.042	0.049	0.06	0.072
P3 [W]	0.012	0.017	0.022	0.033	0.043	0.05	0.062	0.073
Q1[kVAr]	0.014	0.019	0.024	0.036	0.048	0.056	0.068	0.082
Q2[kVAr]	0.014	0.019	0.024	0.036	0.047	0.056	0.069	0.082
Q3[kVAr]	0.014	0.019	0.025	0.036	0.049	0.056	0.068	0.081
Pf1	0.869	0.89	0.9	0.886	0.886	0.9	0.901	0.892
Pf2	0.861	0.885	0.882	0.882	0.884	0.877	0.867	0.874
Pf3	0.893	0.883	0.882	0.894	0.887	0.895	0.91	0.897
N [rpm]	0	0	0	0	0	0	0	0

Table 3-3 shows the average estimated parameters for each frequency and Figure 3-7 and Figure 3-8 show the graphs where the average rotor resistance and rotor/stator inductances vary with frequencies in order to have a better image of the results obtained.

Table 3-3. Average estimated values for blocked rotor test

$f(Hz)$	20	30	40	50	60
$Rs\ (\Omega)$	11,181	14,136	16,942	17,132	16,993
$Ls = \frac{X_s}{2\pi f}\ (\mathrm{mH})$	62,1625	58,0629	55,8180	50,6600	50.6600
$Ls = \frac{X_s}{2\pi f}\ (\mathrm{mH})$	62,1625	58,0629	55,8180	50,6600	50.6600

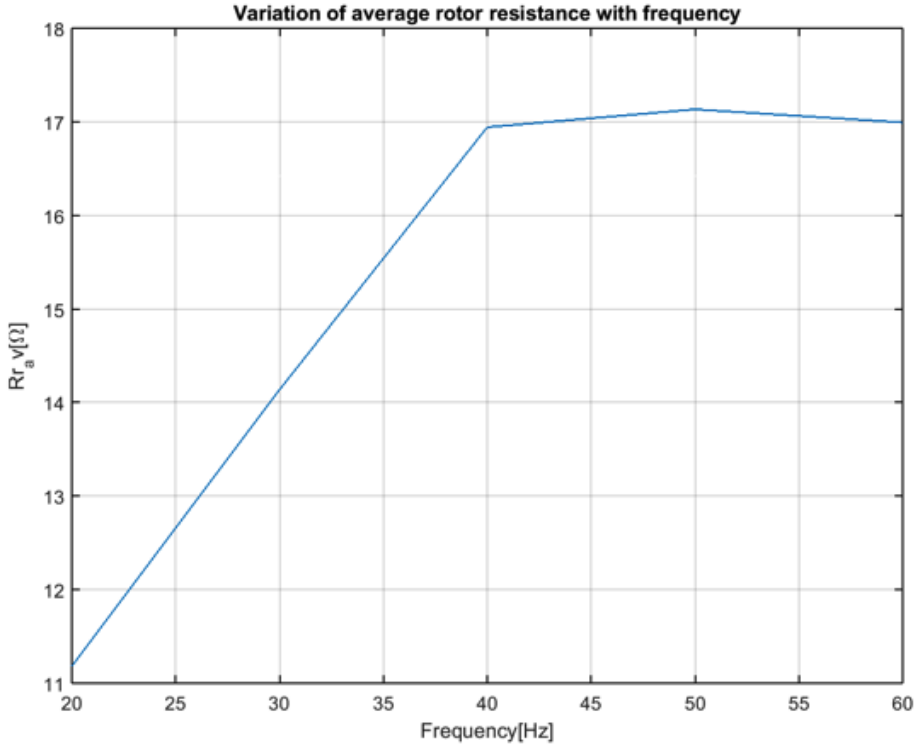

Figure 3-7. Variation of average rotor resistance with frequency

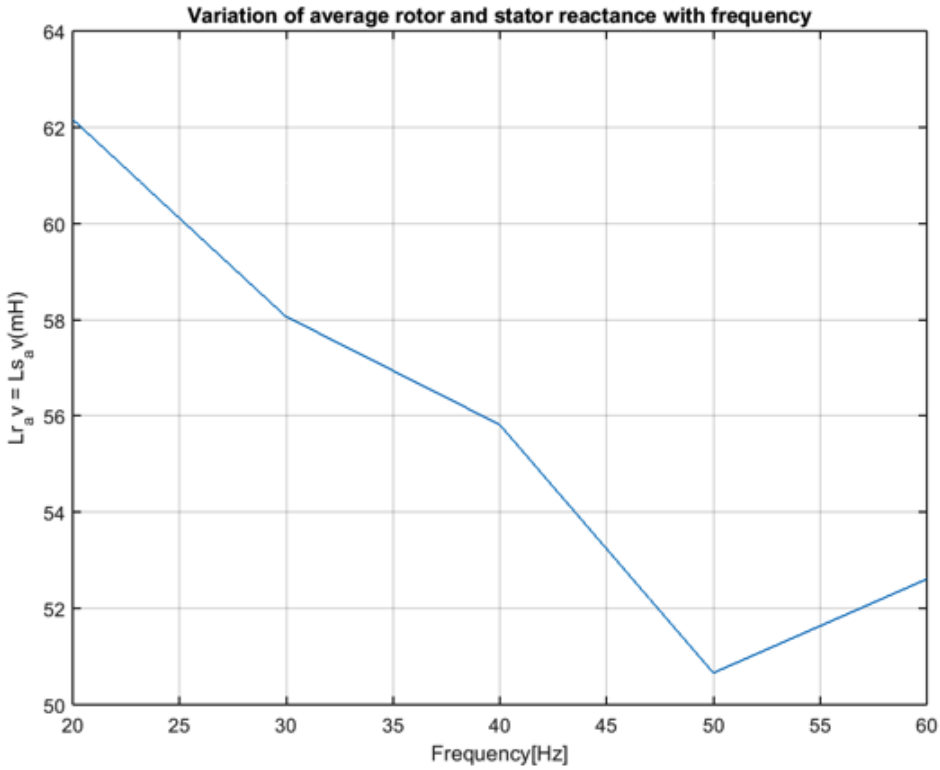

Figure 3-8. Variation of average rotor and stator reactance with frequency

By looking at the results, shown in Figure 3-7 and Figure 3-8, it is clear to see that the parameters change and they change differently. The resistance in Figure 3-6 represents the heating Joule losses from the machine. According to Dente (2007) the Joule losses can be simplified as an approximation to:

$$P_{joule} \propto RI\text{^}2 \tag{3.5}$$

As the frequency of the machine increases, the joule losses increase due to overheating. Although there is an increase in current in this experiment, it is not enough to explain this variation. Thus, to facilitate the understanding of the machine it is made a simplification where the current is almost constant. Having this simplification, it is possible to explain the results depicted in Figure 3-7 where an increase of joule losses directly influences the rotor resistance.

There are significant variations of the parameters, 18% for the inductance value and 34% for the resistance value. However, the values for both stator and rotor resistance are much lower than the core losses, which means they can be neglected in order to create a valid method for this machine in no-grid situation.

The importance of the variation of magnetic flux $\frac{E}{f} = \frac{U_S}{f}$ on the rotor and stator inductance and rotor resistance was also studied and the results are shown in Figure 3-9 and Figure 3-10.

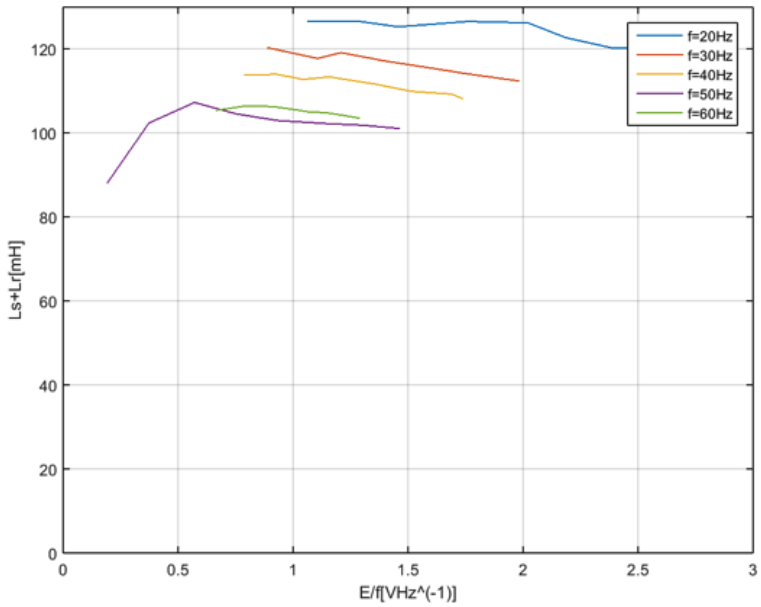

Figure 3-9. Behavior of the Rotor and stator inductance through magnetization variation

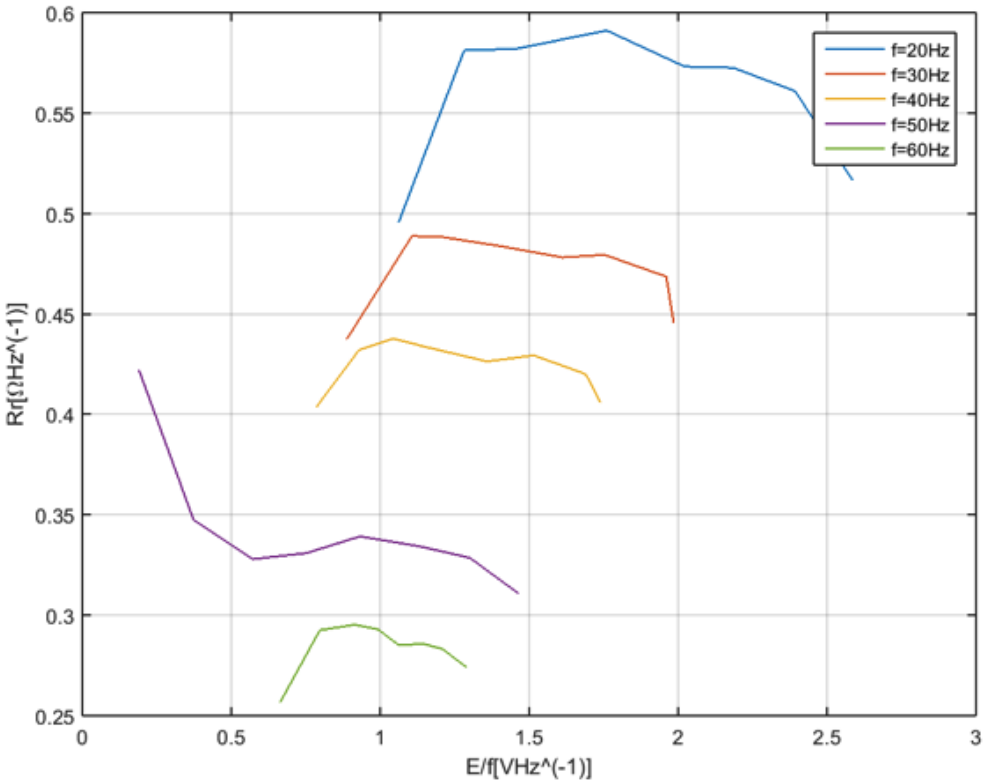

Figure 3-10. Behavior of the rotor resistance through magnetization variation

Figure 3-9 shows the sum of the stator and rotor leakage inductances ($L_s + L'_r$). The values, with a range between $100\,mH\ to\ 130\,mH$, showed that there is no dependence whatsoever with the magnetization level ($^{E}/_{f}$) of the generator. For the electric equivalent circuit, which will be used following sections, it is assumed that they are constant values around 0.11H, and so each inductance as a value of 0.055H.

Concerning the rotor resistance parameter, since it was obtained from the blocked-rotor test, the slip is one and thus the electromotive force induced in the rotor is represented by equation 3.6.

$$E = [R'_r + (j2\pi f L'_r)]I'_r \tag{3.6}$$

Dividing all the parameters, it is possible to get the effect of magnetization in both R'_r and L'_r and equation 3.6 becomes equation 3.7.

$$\frac{E}{f} = [\frac{R'_r}{f} + (j2\pi L'_r)]I'_r \tag{3.7}$$

From here, the magnetization is divided into real part and imaginary part and that the imaginary part is the leakage flux that cannot be used to link the stator and the rotor (Equation 3.8).

$$\phi_{leakage} = \frac{E}{f} = j(2\pi L_{'r})I_{'r} \tag{3.8}$$

This fact is the reason why the rotor and stator leakage inductance are not influenced by the magnetic flux, because the magnetic flux remains constant and all the variations of the flux affect directly the rotor current. The real part of Equation 3.7, also called as the useful magnetic flux, is the flux that links the rotor with the stator $\phi_{linkage} \approx \frac{R'_r}{f} I_{'r}$. This linkage flux is going to help understand how $\frac{R'_r}{f}$ changes with $\frac{E}{f}$. It was already stated that the leakage flux remained approximately constant with the magnetization. Equation 3.9 is the equation that characterizes the magnetic flux and its separation in linkage magnetic flux and leakage magnetic flux.

$$\frac{E}{f} = \left[\frac{R'_r}{f} + (j2\pi L_{'r})\right] I_{'r} \;\leftrightarrow\; \phi_{\mathrm{m}} = \phi_{linkage} + \phi_{leakage} \tag{3.9}$$

During the experimental work, it was possible to acquire that the rotor resistance shall remain approximately constant because every increase of the magnetization level is compensated with a proportional increase of rotor current. Therefore, it is seen in both graphs, in Figure 3-9 and Figure-3,10, that for a variation of the magnetization level there is small variation of the parameters.

3.1.2. No-load Tests

In this experiment, the rotor is not connected to the load, and so it is an open circuit. This was the method applied because it is meant to find the parameters in the magnetization branch. The objective was, for each frequency, to increase the value of SG voltage until the rotor current reaches its nominal value. For each voltage were set 8 points with different field voltage,V_f, of the SG. These field voltages values vary between an interval of $V_f(20hz{:}\,60Hz){:}\;\alpha\,[50;400][V]$.

The no-load test, like the open circuit test on a transformer, gives information about exciting current and rotational losses (Dente, 2007a). The machine will rotate at almost a synchronous speed, which makes slip nearly zero. As it shows Figure 3-11, the no-load equivalent of induction machine is again simplified. However, this time the secondary branch is the one to be neglected.

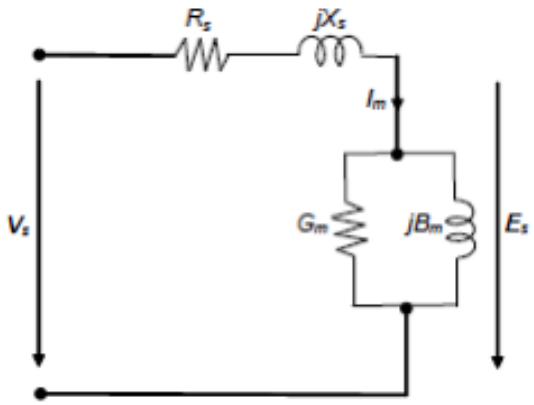

Figure 3-11. Equivalent circuit of the no-load machine (Paiva, 2011)

There are two different ways of calculating the core inductance and the core resistance. The difference between them is whether it is considered the resistance and inductance from the stator branch or not. The equation (3.6), where it is considered the parameter R_s, represents the iron losses, which are the quotient between the square open-circuit voltage and the difference between the open circuit power and the stator Joule losses. Equation (3.8) is very similar, however it does not consider the effect of Joule power losses. Equation (3.7) is the determination of the magnetic inductance that is the quotient between the square open-circuit voltage and the Leakage stator power losses. Finally, Equation (3.9) is Equation (3.7) without the Joule power losses (Paiva, 2011):

$$R_m = G_m = \frac{{U_{0avg}}^2}{(P_{0avg} - {I_{0avg}}^2 * R_s)} \tag{3.6}$$

$$X_m = B_m = \frac{{U_{0avg}}^2}{(Q_{0avg} - {I_{0avg}}^2 * X_s)} \tag{3.7}$$

$$R_m = G_m = \frac{{U_{0avg}}^2}{(P_{0avg})} \tag{3.8}$$

$$X_m = B_m = \frac{{U_{0avg}}^2}{(Q_{0avg})} \tag{3.9}$$

Being U_0 the average 3-phase no load stator voltage, I_0 the average 3-phase no load stator current and P_0 and Q_0 the respective average no load active and reactive power. In this thesis the first ones are chosen, because it is important to choose the Joule Power Losses for a more efficient determination of the electrical parameters and how to control its losses.

To perform the tests with the induction machine it is required to measure the 3-phase currents, the 3-phase voltages, the active power, the apparent power, the power factor and the speed. The obtained results for 20 Hz are shown in Table 3-4. The tests for other frequencies are displayed in Annex B.

Table 3-4. Results of the No-Load test for 20Hz frequency

Uc [V]	54,5	65,2	75,8	85,2	95	105	120	132
U1 [V]	31,4	37,5	43,8	48,8	54,8	60,6	71,7	76,7
U2 [V]	30,9	37	43	48,1	53,7	59,6	70,5	75,4
U3 [V]	31,2	37,3	43,3	48,9	54,4	60	70,9	75,9
I1 [A]	0,36	0,43	0,51	0,58	0,66	0,74	0,91	0,99
I2 [A]	0,35	0,42	0,5	0,57	0,65	0,72	0,89	0,97
I3 [A]	0,36	0,43	0,51	0,59	0,68	0,74	0,92	1,01
P1 [kW]	0,005	0,006	0,008	0,01	0,013	0,015	0,022	0,026
P2 [kW]	0,004	0,005	0,007	0,009	0,011	0,013	0,018	0,021
P3 [kW]	0,004	0,006	0,008	0,009	0,012	0,014	0,02	0,024
Q1 [kVAr]	0,011	0,016	0,022	0,029	0,038	0,045	0,065	0,076
Q2 [kVAr]	0,011	0,015	0,021	0,028	0,036	0,043	0,063	0,073
Q3 [kVAr]	0,011	0,016	0,022	0,029	0,038	0,044	0,065	0,077
Pf1	0,401	0,377	0,345	0,343	0,335	0,33	0,336	0,339
Pf2	0,384	0,339	0,313	0,31	0,302	0,295	0,29	0,289
Pf3	0,388	0,351	0,329	0,327	0,311	0,309	0,308	0,313
N [rpm]	395	399	396	395	400	400	400	408

Although it was made an average approximation for the blocked rotor parameters, it is not possible to take average values for R_m and L_m. This happens since the 8 points that were measured through each frequency are very disperse from each other, preventing it from having accurate comparison between frequencies. So, the solution found for this problem was to, instead of tackling both frequency and voltage as separate things, combine them in the $\frac{V}{f}$ command, where it is possible to control one of them as a function of the other.

In the next table (Table 3-5) it is shown the average results for the magnetizing inductance and the core losses for $20Hz$. The four remaining tables can be seen in Annex D.

Table 3-5. Estimation of L_m and R_m on 20Hz frequency

$\frac{U_{savg}}{f}$	1,558	1,863	2,168	2.43	2,715	3,003	3,552	3,8
$R_m(\Omega)$	357,81	460,50	586,13	611,33	715,85	760,95	860,46	888,50
$L_m = \frac{X_m}{2\pi f}\ (mH)$	602	603	590	575	560	563	536	523

In the figures below (Figure 3-12 and Figure 3-13) it can be seen the response of both the magnetizing inductance and the core losses with the $\frac{E}{f}$.

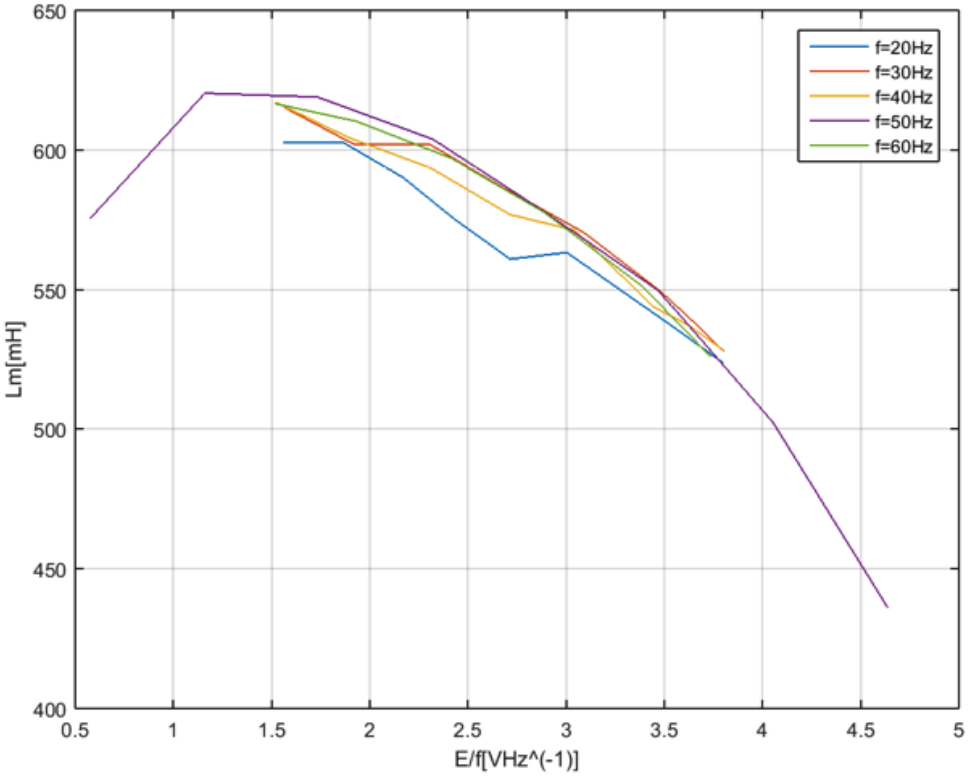

Figure 3-12. Evolution of the Magnetic inductance with $\frac{E}{f}$

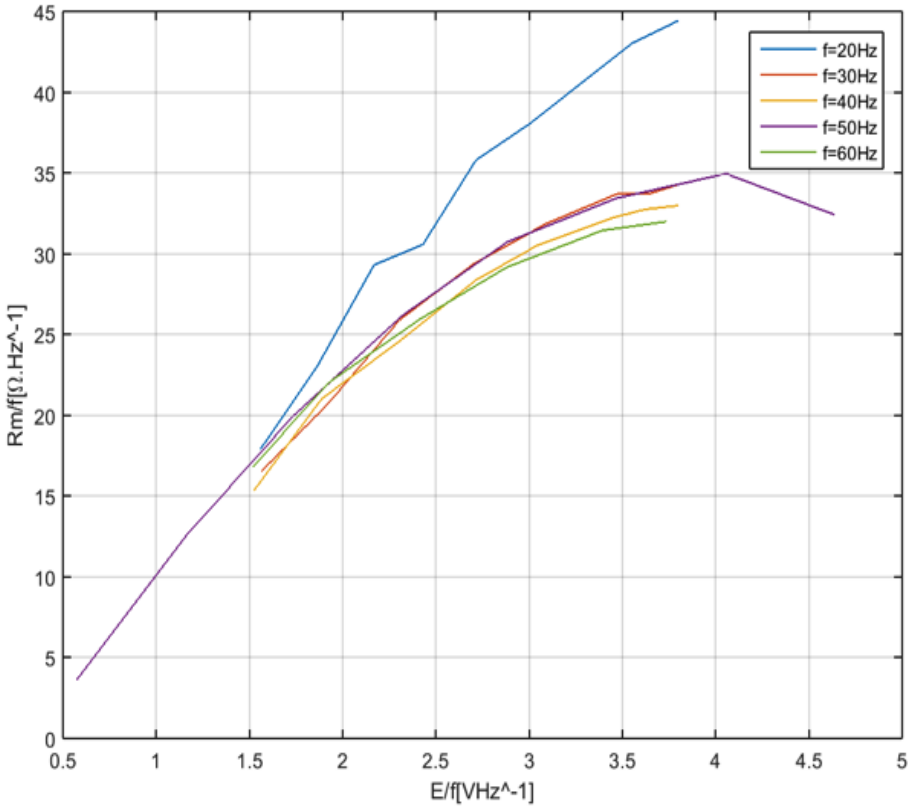

Figure 3-13. Evolution of the core losses with $\frac{E}{f}$

The results presented in the previous figures show a big variation for both core losses and magnetization inductance. In the frequency domain, the loss separation among the static hysteresis, classical eddy current and excess loss is widely used. These iron loss components are calculated in terms of the $\frac{E}{f}$ peak flux density, and the material dependent coefficients k_h and k_e, respectively. However, it is hard to quantify those losses and the best approximation for both losses is found in this next equation:

$$P_m = k_h * (\frac{E}{f}) * f + k_e(\frac{E}{f}) * f^2 = P_h + P_e \tag{3.10}$$

The elements of this equation are:

- k_h, hysteresis coefficient or Steinmetz Coefficient;
- $\frac{E}{f}$, maximum flux density ($\frac{V}{Hz}$);
- f, electrical frequency (Hz);
- k_e, eddy current constant;
- P_m, magnetization power;
- P_h, hysteresis losses Power;
- P_e, eddy current losses Power

It can be seen in Figure 3-13 a proportional increase of magnetization resistance, R_m, with the increase of magnetization flux. It is known that the magnetization power can be described as:

$$P_m = \frac{E^2}{R_m} = \frac{E^2}{f}\frac{f}{R_m} \tag{3.11}$$

Joining equation equations 3.10 and 3.11, the connection between $\frac{R_m}{f}$ and $\frac{E}{f}$ can be found, as shown in equations 3.12 and 3.13.

$$P_m = \frac{E^2}{R_m} = \frac{E^2}{f}\frac{f}{R_m} = k_h\left(\frac{E}{f}\right)f + k_e\left(\frac{E}{f}\right)f^2 \leftrightarrow E\frac{f}{R_m} = k_h f + k_e f^2 \tag{3.12}$$

$$\frac{R_m}{f} = \frac{E}{k_h f + k_e f^2} \tag{3.13}$$

As it is known, the Eddy current losses are much smaller compared with the hysteresis ones, which allows transforming Equation 3.13 into Equation 3.14, which verifies the assumption that for an increase in the magnetic flux there is a proportional increase in the core losses.

$$\frac{R_m}{f} = \frac{E}{k_h f} \tag{3.14}$$

3.2. DC Motor

Although the DC motor is not a parameter of the induction machine, it is necessary to give some background for this component due to its role as a prime mover in the experiment. The axis of the DC machine and the induction machine are the same, which helps to realize the importance of a brief review of the DC machine. Therefore, an analysis of the DC machine was important for the study of its power losses in order for a better study of the efficiency of the DC motor.

Its equivalent circuit for steady state condition is simpler to estimate. As shows Figure 3-14, both armature and field circuits can be described as a resistance, in steady state operation. The values of these resistances can be determined, using a digital multimeter in the terminals of both circuits, which are shown in the same figure.

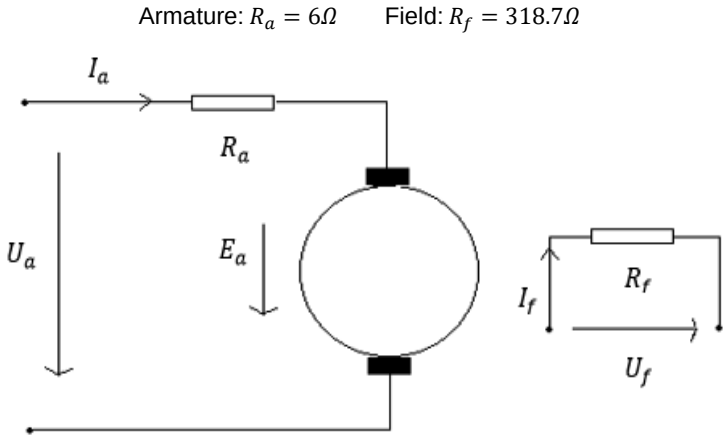

Figure 3-14. DC Motor's equivalent circuit - separate excitation case (Dente, 2007b)

The nameplate information regarding the DC motor is shown in Table 3-6.

Table 3-6. Nameplate information of the DC machine

DC Machine	
Armature Voltage	230 V
Armature Current	4.4 A
Nominal Speed	1500 rpm
Nominal Power	1 kW
Field Voltage	220 V
Field Current	0.55 A

Finally, the main point was to analyze the DC motor and its losses. Considering the case of separate excitation, shown in Figure 3-14, the DC Motor steady state conditions is expressed by the following set of equations (Dente, 2007b):

$$I_f = \frac{U_f}{I_f} \tag{3.15}$$

$$U_a = R_a * I_a + k_\emptyset * \emptyset_u(I_f) * w_r \tag{3.16}$$

$$k_\emptyset \emptyset_u(I_f) * I_a = T_c \tag{3.17}$$

$$T = -\frac{(k_\emptyset \emptyset_u)^2}{R_a} * w_r + \frac{U_a}{R_a} * k_\emptyset \emptyset_u \tag{3.18}$$

The power flow in the DC Motor, in a more simplified form, can be expressed by equations (3.19), (3.20) and (3.21).

$$P_{IN} = U_a * I_a + U_f * I_f \tag{3.19}$$

$$P_{LOSS} = R_a * {I_a}^2 + R_f * {I_f}^2 + P_{rot\_loss} \tag{3.20}$$

$$P_{rot\_loss} = P_{IN} - P_{LOSS} \tag{3.21}$$

In equation (3.20), the losses by Joule effect in R_a and R_f can easily be determined because they only depend on the values of armature and field currents, measured during the tests. On the other way, the rotational losses P_{rot_loss} are not easy to determine. For this experiment, an approximate estimation was made by testing the DC Motor for no load conditions. In no load conditions, all of the power measured in armature and field are losses. Therefore, by separating the Joule losses from the rotational losses (mechanical and magnetic), an estimation of the last ones can be achieved.

Therefore, for no load conditions the resultant equation (3.22) comes from joining equations (3.20) and (3.21).

$$P_{rot\_loss} = P_{IN} - (R_a * {I_a}^2 + R_f * {I_f}^2) \tag{3.22}$$

3.3. Chapter Conclusions

The work performed in this chapter had the purpose of analyzing the behavior of the parameters of the induction machine while being induced with the variation of different frequencies and voltages, a situation that is very common in a PAT system in a hydraulic application. This study is going to be a very useful tool to get a better understanding of how the induction machine can work under off-Grid situations. To estimate and understand the parameters of the induction machine, it was briefly studied its electrical equivalent system and deeply understood what each parameter represents. These parameters are not resistances and inductances that are part of the machine, but they represent a mathematical approach for better understanding the physical phenomena that happens in the induction machine.

With the results presented in this chapter, it was made clear that the electrical parameters of the induction generator are heavily influenced by the frequency and by the magnetization level. The rotor Joule Losses and the leakage losses from both the stator and the rotor are not particularly affected with the magnetization level. However, they can be influenced by a sudden change in the frequency as it was shown in the blocked rotor tests. For the magnetization parameters it was observed that they are sensible to frequency and magnetization variations, which is a very important conclusion for the development of a more accurate induction generator model. Magnetization parameters, especially the magnetization leakage, are going to be the key element for determining an analytical model and a simulation one, which will be studied in the following chapters. This model will help to improve the global efficiency of the SEIG system.

4. The Self-Excited Induction Generator in Off-Grid operation

In this chapter, it is going to be studied with more detail the off-grid operation of the Self-Excited Induction Generator (SEIG). This analysis is divided into two three parts:

1. A theoretical analysis of the SEIG aiming to find the proper dynamic equations to determine the minimum possible capacitance values for different resistive loads and different rotational speeds;
2. Development of a numerical model that replicates the behavior of the SEIG under off-grid conditions and the numerical validation of results obtained analytically in 1);
3. Experimental testing of the determined minimal capacitance values in 1) and 2) to compare both simulation and experimental results, in order to validate the numerical model;

The squirrel-cage induction machine as generator remains unquestionably the one that is most widely spread for off-grid hydro energy conversion applications for reasons of robustness and price. Its structure without carbon brushes and permanent magnets gives it unparalleled robustness and longevity, with acquisition and maintenance costs much lower than that of another type of generator of the same power. Finally, the squirrel-cage induction machine is very tolerant to extreme operating regimes (overspeeds, overloads, *etc*).

A different aspect about its operation as generator consists of presenting a voltage whose amplitude and frequency are, in the case of off-grid operation, very sensitive to variations in speed and load. Moreover, the induction generator provides active power but always need to absorb the reactive power necessary for its magnetization, which is its main drawback. Only a system based on an induction machine with a capacitor self-excitation using a capacitor bank directly connected to a load makes it possible to obtain a purely autonomous operation. On the other hand, the phenomenon of self-excitation is difficult to control because the load variations directly affect the values of the voltage and the frequency delivered.

In order to determine the performance and operating limits of SEIG system, the complete equivalent-circuit per phase of the induction machine is first used to calculate the minimum capacitance values for the SEIG system. Follow, dynamic simulations of the SEIG system plus its load are performed and validated by experimental tests using a model of the induction generator now established in *d-q* coordinates.

The main features of the analysis that are going to be done in this chapter are schematized in Figure 4-1 where a star-connected capacitor bank is placed between the load and the induction machine, in order to supply reactive power that is necessary to its magnetization.

In Figure 4-1, a *prime mover* represents the hydraulic turbine, which supplies a mechanical power to the induction machine. Due to that, a small voltage appears first in the stator coils with a frequency proportional to the rotor speed, due to residual magnetism present in the machine from previous utilizations. Its iron core never stops being magnetized from previous operations and helps the machine to get a faster magnetization. With this initial voltage, the capacitor bank produces current, providing reactive power, *Q*, increasing the stator voltage and increasing the magnetization level of the machine. Follow, the “self-excitation” of the machine halts due to the magnetic saturation of the iron core.

The induction generator begins to supply active and reactive power (coming from the bank of capacitors) to feed the specific load. However, it must be noticed that the generator consumes also part of the reactive power available. This is the main problem of a SEIG system and its bank of capacitors: the need for feeding both machine excitation and the load.

There is another difficulty to account for a SEIG system in an off-grid scenario: the set of loads that are directly powered by the generator can be very different from each other, having different power needs, for example. This can be very dangerous for generator operation because the capacitors values need to change according to the load, which makes the frequency and voltage in the SEIG system very unstable for the safety of the induction generator. Despite, a change in the load will also influence the generator frequency (the synchronous speed, and so the rotational speed) and stator voltage.

In this work, a star connection was chosen for the simulation designs. In this section and throughout the course of this thesis, the general type of load considered was R purely resistive as it was used in the laboratory.

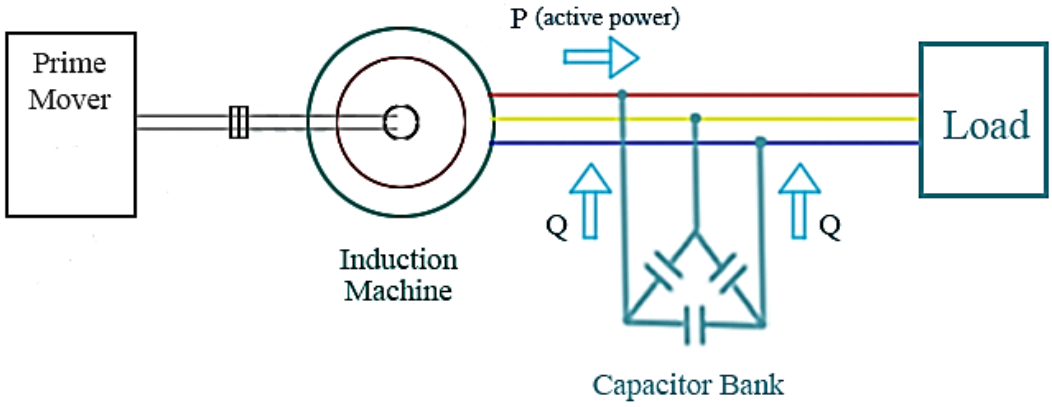

Figure 4-1. Self-excited induction generator system (Capelo, 2017)

4.1. Theoretical analysis

This section analyzes the off-grid SEIG system using its complete electrical equivalent circuit studied in Chapter 3, together with the parameters relations obtained as function of the voltage and frequency signals of the generator. With the equivalent circuit, it will be possible to determine the equations for the minimal capacitance values of the SEIG as functions of its speed and magnetization level. In order to do this, a numerical model was created and the software Maple was used as a support tool for mathematical algebra.

4.1.1. Problem identification and proposed solution

The work performed in this chapter and further sections was adapted from the previous work performed by (Capelo, 2017; Capelo et al., 2017), with appropriate adjustments. That off-grid SEIG system not only supposed that the parameters of the electrical equivalent circuit of the induction generator were constant, being the same as the parameters obtained for the rated frequency and voltage, but also neglected the iron core losses. While it can be a possible assumption with relative accurate results, it can also bring some problems for the SEIG functionality where minimal capacitance values can be under or overestimated for the off-grid operation of the SEIG, as also pointed out in those works. It was concluded that there are two hypotheses under which the equivalent circuit model was based upon (Capelo, 2017; Dente, 2007c):

1. The assumption that the electrical circuit parameters that really represent the rotor losses of the induction generator are time-invariant, being irresponsive to any operating frequency and stator voltages, and;
2. The negligence of the iron core losses, which was shown in Chapter 3 that they change significantly while operating out of the rated conditions;

These two hypotheses must be considered not only to analyze a more accurate behavior of the SEIG to reach a best efficiency in the recovery system, but also to protect the machine itself. With this over and under estimation, two situations may arise:

1. By underestimating the capacitance values, the capacitor bank is not able to give the necessary reactive power and so the machine never starts to operate and supply the load with power, and;
2. By overestimating the capacitance values, the capacitor is giving to much reactive power, which for rated frequency and voltages, the torque produced in the machine is higher than the rated one. Thus, by giving too much reactive power, the machine has a significant higher rotational speed that it is intended to. It means that the machine can suffer from an overflow of work, which can reduce its working age or worse, it can destroy the machine.

To summarize, the objective in the following sections is to develop a model considering that does not consider both assumptions.

4.2. Analytical model

The minimum capacitance needed to keep the generator excited without a load can be easily determined by analyzing the magnetizing curve of the induction machine that can be obtained experimentally (Chan, 1993). However, when a load is applied, the capacitance values must change, depending not only on the parameters of the machine, but also on the load applied to the system and the rotational speed of the generator. Therefore, before starting testing the machine or even assemble the system, it would be convenient to have an equivalent circuit model including the induction machine and the load in question, which will allow making a first estimation of the range of minimum capacitances.

In this section, it was developed a general analytical model for the per-phase SEIG circuit that allows determining the range of the capacitances required. As Abbou, Barara, Ouchatti, Akherraz, & Mahmoudi (2013) and Capelo (2017) determined, the best approach for this case is the Nodal Admittance approach where one determines the equations through the main nodes in the system that are: the load, the capacitor bank and the induction generator nodes.

There are other alternatives, such as the Loop Impedance approach, which was used by Eltamaly (2002) and Valadão (2012). Its main goal is to, instead of studying the admittance through the nodes of the system, use the loops of the system in order to find the respective impedances. This is a more direct approach than the Nodal Admittance Approach however, since parallel admittances sum to each other, the Nodal approach is the chosen for this work because the calculations are easier to do. The approach developed in this thesis begins adding the core losses effect in the equivalent circuit of the induction generator. Core losses will be represented by a magnetizing resistance $R_m$put in parallel with the magnetizing inductance L_m. Although this is the main difference between the work developed previously, the change considered in the equivalent circuit has a significant impact on the mathematical calculations, becoming more complex.

The per-phase equivalent circuit of a SEIG system is shown in Figure 4-2. As it can be seen, there are three main components in this circuit:

- The inductive load (R_L, X_L);
- One phase bank of capacitors or the reactance (X_C);
- Equivalent electric circuit of the induction generator;

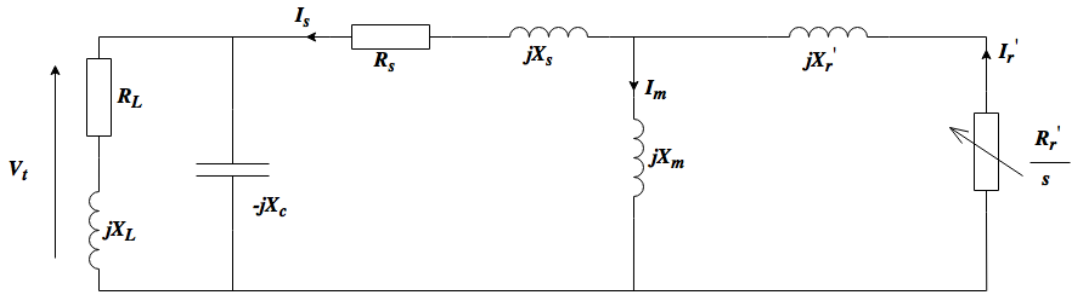

Figure 4-2. Equivalent electric circuit of the self-excited induction generator connected to the load
(Fernandes et al., 2018)

From the analysis performed in Chapter 3, it was observed that the electrical frequency can be different from the rated frequency, $f_N = 50\ Hz$, and so it is necessary to normalize all the parameters to the same electrical frequency (per-unit frequencies). This is obtained by dividing all the parameters per unit frequency, $a = \frac{f}{f_N}$ p.u. Equations 4.1 and 4.2 show how to determine the per unit frequency:

$$a = \frac{w}{w_s} = \frac{\frac{2\pi f}{p}}{\frac{2\pi f_N}{p}} = \frac{f}{f_N} \tag{4.1}$$

$$b = \frac{w_r}{w_s} = \frac{N_r}{N_s} = \frac{N_r}{60\frac{f_N}{p}} \tag{4.2}$$

The slip s is defined as the difference between the synchronous speed, $\boldsymbol{w}$, and its mechanical speed, w_r, $s = \frac{w - w_r}{w}$**.** Using equations (4.1) and (4.2) it is possible to transform the slip as a function of the per-unit frequency a. Such expression is shown in equation 4.3, where b is the per-unit speed:

$$s = \frac{w - w_r}{w} = \frac{\frac{w}{w_s} - \frac{w_r}{w_s}}{\frac{w}{w_s}} = \frac{a - b}{a} \tag{4.3}$$

For an electrical quantity, the frequency can be expressed as $f = a\, f_N$, with all reactances given by equations (4.4) – (4.8).

$$X_s = 2\pi(af_N)L_s \tag{4.4}$$

$$X_r' = 2\pi(af_N)L_r \tag{4.5}$$

$$X_m = 2\pi(af_N)L_m \tag{4.6}$$

$$X_L = 2\pi(af_N)L_L \tag{4.7}$$

$$X_C = \frac{1}{2\pi(af_N)C} \tag{4.8}$$

Finally, by dividing all the parameters by a, it can be obtained the normalized reactances with the per-unit frequency:

$$\frac{X_s}{a} = 2\pi f_N L_s = X_{s_N} \tag{4.9}$$

$$\frac{X_r}{a} = 2\pi f_N L_r = X_{r'_N} \tag{4.10}$$

$$\frac{X_m}{a} = 2\pi f_N L_m = X_{m_N} \tag{411}$$

$$\frac{X_L}{a} = 2\pi f_N L_L = X_{L_N} \tag{4.12}$$

$$\frac{X_c}{a} = \frac{1}{2\pi a^2 f_N C} = \frac{X_{C_N}}{a^2} \tag{4.13}$$

$$\frac{\frac{R_r'}{s}}{a} = \frac{R_r' a}{a(a-b)} = \frac{R_r'}{a-b} \tag{4.14}$$

Figure 4-3 gives the simplified equivalent SEIG per phase circuit based on the per-unit frequency a:

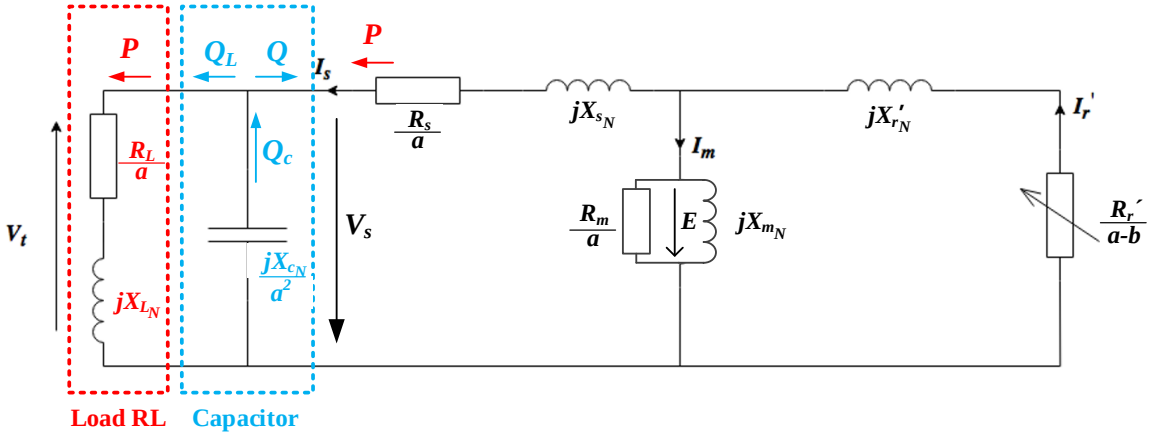

Figure 4-3. Updated equivalent circuit of the self-excited induction generator connected to the load with all parameters replaced by the equations (4.9) to (4.14).

Applying the Nodal Admittance approach to the terminal voltage, V_t, and with the help of Kirchhoff first law, the sum of all currents in one node is equal to zero (4.15). Using the simple circuit approximation, where Y_t is the sum of all the admittances in the circuit, load (Y_L), capacitor (Y_C) and induction generator (Y_{IN}) ones, it is possible to determine equation (4.16).

$$\frac{V_t}{a} \cdot Y_t = 0 \tag{4.15}$$

$$Y_t = Y_{IN} + Y_L + Y_C \tag{4.16}$$

From equation (4.15) it can be said that to assure the self-excitation of the induction generator, the total admittance of the equivalent circuit must be zero. In equation (4.16), Y_{IN} represents the total

admittance from the induction generator. Y_L is the load admittance and Y_C is the capacitor admittance. This equation must be seen from the point of view of the load for equation (4.16) to be valid. From the previous equations (4.9 – 4.14) and by observing figure 4.4, it is possible to state the expressions for all admittances as:

$$Y_C = -\frac{a^2}{jX_C} \tag{4.17}$$

$$Y_L = \frac{1}{\frac{R_L}{a}+jX_L} \tag{4.18}$$

$$Y_m = \frac{1}{\frac{R_m}{a}} + \frac{1}{jX_m} = \frac{a}{R_m} - \frac{j}{Xm} \tag{4.19}$$

$$Y_r = \frac{1}{\frac{R_r{'}}{a}+jX_r{'}} \tag{4.20}$$

$$Y_s = \frac{1}{\frac{R_s}{a}+jX_s} \tag{4.21}$$

$$Y_{IN} = \frac{Ys(Yr+Ym)}{Ys+Yr+Ym} \tag{4.22}$$

Finally, the total admittance of the system, which has a significant level of complexity, becomes given by expression (4.23-4.24).

$$Y_t = \frac{-a}{jX_c} + \frac{1}{\frac{R_L}{a}+jX_l} + \frac{1}{Z_{IN}} = 0 \tag{4.23}$$

$$Z_{IN} = \left(\frac{R_S\left(\frac{1}{\frac{R_{R'}}{a-b}+jX_{r'}}+\frac{a}{R_m}-\frac{1}{X_m}\right)}{a\left(\frac{1}{\frac{R_{R'}}{a-b}+jX_{R'}}+\frac{a}{R_m}-\frac{1}{X_m}\right)} + jX_s\left(\frac{1}{\frac{R_{R'}}{a-b}+jX_{R'}}+\frac{a}{R_m}-\frac{1}{X_m}\right)\right)\left(\frac{1}{\frac{R_S}{a}+jX_s}+\frac{1}{\frac{R_{R'}}{a-b}+jX_{r'}}+\frac{a}{R_m}-\frac{1}{X_m}\right) \tag{4.24}$$

Finally, it is necessary to separate the real values from the complex ones from equation (4.15-4.16), and thus a new set of equations is required:

$$Re\{Y_t\} = 0 \tag{4.25}$$

$$Im\{Y_t\} = 0 \tag{4.26}$$

With this separation of real and imaginary part of the total admittance, two equations were obtained. Due to its independence from the values of the capacitance, and because Y_c is a pure imaginary value, the real roots of the equation (4.25) are responsible for determining the value of the per-unit frequencies, which these same roots are going to determine the imaginary roots of (4.26) that are responsible to determine the minimal capacitance values for a determined frequency.

From the decomposition of equation (4.23), it is acknowledged that the only way for determining its roots is if the numerator is equal to zero. Thus, the only necessary part of the equation is the

numerator. For both equations (4.25) and (4.26), it is necessary to calculate parameters D_k, B_k, A_k. Coefficients D_k are the values from numerator of (4.25), which are function of a specific per-unit frequency a_k. Coefficients B_k, A_k are the equations that are function of a specific per-unit frequency a_k that helps determining the capacitor inductance X_c.

It has come to the attention that instead of having only four possible roots for *a* in equation (4.25), as Capelo, 2017 previously determined , the complexity of the polynomial has increased from 4 to 6 possible roots with the addition of the core losses in the model through the R_m parameter. For these 6 possible roots, a_k, only the ones who are purely real can be used in equation (4.26) because only real roots correspond to steady-state operations.

$$D_6a^6 + D_5a^5 + D_4a^4 + D_3a^3 + D_2a^2 + D_1a^1 + D_0 = 0 \tag{4.27}$$

$$X_{C_N} = -\frac{A_8a^8+A_7a^7+A_6a^6+A_5a^5+A_4a^4+A_3a^3+A_2a^2+A_1A+A_0}{B_6a^6+B_5a^5+B_4a^4+B_3a^3+B_2a^2+B_1a+B_0} \tag{4.28}$$

$$C_k = \frac{1}{2\pi f_N a_k X_{C_N}},\ k = 1, \dots, 8 \tag{4.29}$$

Equation (4.29) allows the calculation of the minimal capacitance value that can excite the induction generator. Equation (4.30) determines the coefficient D_6, which is one of the terms from equation (4.25) that are related to the per-unit frequency to the sixth power, a^6. The remaining equations to determine the rest of the D_k coefficients can be seen in the annex E.

$$D6 = Xm\text{^}2Xr\text{^}2 * \left((Rm + Rs) * Xl^2 + Rl * Xs^2\right) \tag{4.30}$$

With the equation (4.30) and the ones regarding the D coefficient in annex E, (E.1 to E.5), it is possible to obtain the per-unit frequency $a_l, l = 1, \dots, 6$. From this are extracted the only purely real solutions for a. These values are then put in equation (4.28). Equation (4.31-4.32) represent, respectively, the coefficients A_8 and B_6. The remainder B_k and A_j coefficients are found in Annex E.

$$A_8 = {X_L}^2 * {X_m}^2 * {X_r}'^2 * {X_s}^2 \tag{4.31}$$

$$B_6 = {X_m}^2 * {X_r}^2 * X_s * (X_s + X_L) \tag{4.32}$$

Equations (4.27) and (4.28) allowed to calculate $C_K, k = 0,1, \dots, 6$ using (4.29). However, these calculations are not a linear process because the parameters of the induction generator may change with diverse degrees for different operating points. Thus, it is important to elaborate an advanced version of the previous analytical methodology, capable of including the change of machine parameters according to its operating point.

4.2.1. New Numerical Algorithm to Calculate C_K values

To compute the electrical parameters, the voltage and electrical frequency of the machine, which depends on the electrical parameters, must be known. A new numerical algorithm was developed, which a flowchart of the code is shown in

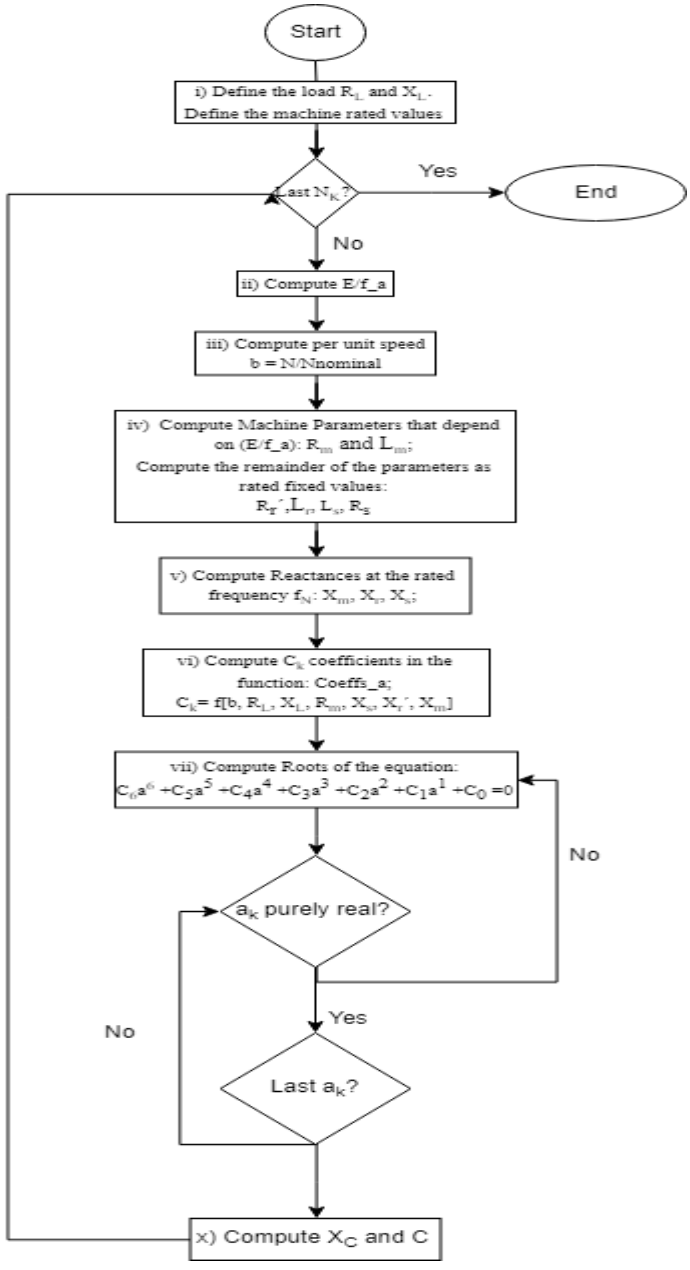

Figure 4-4. In this model, the electrical reactance must be defined at the rated frequency of the induction generator.

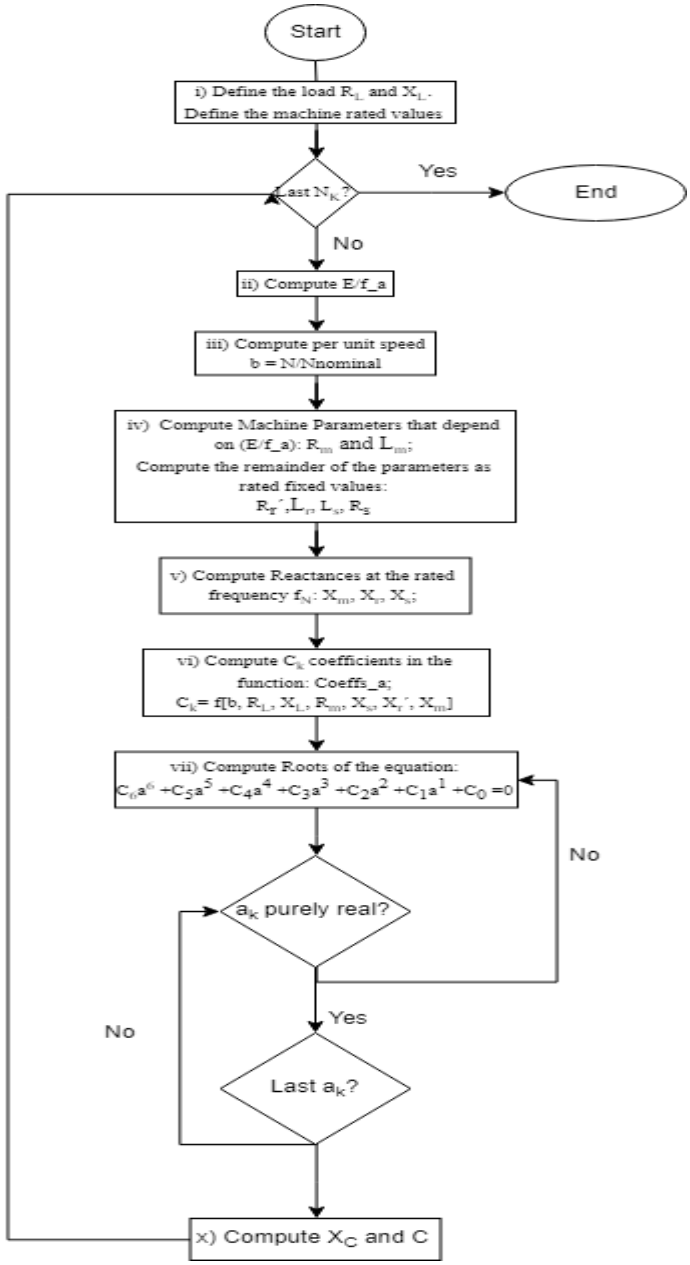

Figure 4-4. Flowchart of the new algorithm for determination of minimal capacitance values.

The algorithm starts in step i) where the load electrical parameters (i.e., R_L and X_L) are defined. After establishing the range of different speeds that the generator will operate commanded by the hydraulic turbine, a closed-loop begins where steps from ii) to xi) are repeated until all a_k values associated with the speed value N_k are computed. This loop keeps running until all the range of speeds are swept. The loop starts in step ii) where it is computed the rated magnetic flux of the machine, with $\frac{E}{(f/a)}$. Then through steps iii) to ix) are made the needed requirements to find all the six possible frequencies f_k.

Step iii) is where is determined the per unit speed, b $[p.u.]$, and through steps iii) to v) the electrical parameters of the SEIG are computed, namely, parameters R_m and L_m with their dependence upon the rated magnetization given by $\frac{E}{(f_k)}$. In step iv), the remaining parameters are considered constant at their original rated values.

Step vi) is necessary to determine the D_k coefficients of the equation (4.25). Follow, in step vii) is where the algorithm determines the roots of step vi). After that, the algorithm calculates all the six frequencies that could be used in the computation of the X_C and the C_{min}, the minimal capacitance values-

At last, having all the six frequencies been calculated, the algorithm enters in a new loop within the loop where each frequency is going to be swept. Before step x), there is a logical test to be passed and it is to check if the frequencies are purely real. With the last of those, it is now possible to calculate X_C and C. After passing this loop, it is determined the least capacitance value available.

4.2.2. Comparison between algorithms to calculate C_K values

In this section, the results for the minimal capacitance will be analyzed and a comparison will be made between an analytical model with iron losses and variable electrical parameters with rated magnetization and with a model without those specifications. It was chosen only a pure resistive load because when the experimental work done for the determination of electrical parameters was made, the inductive load was not used. Figure 4-5 to Figure 4-7 show the difference between two methodologies of the off-grid SEIG, one without the concern for the iron losses, represented by the red line, and the other where the R_m is taken into consideration, represented by the black line.

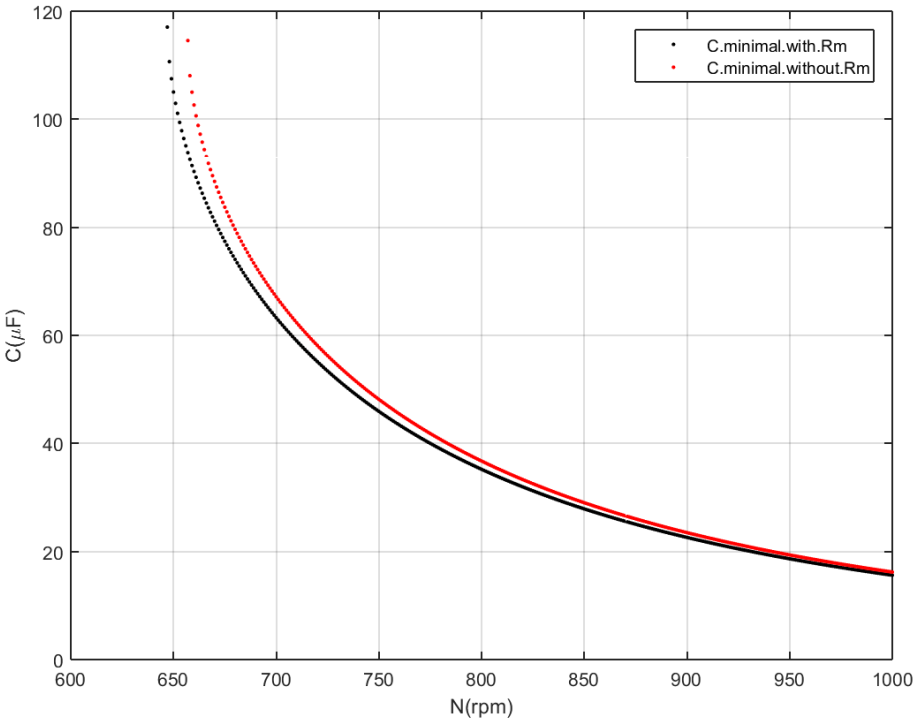

Figure 4-5. Minimal capacitances to excite the SEIG for R_L = 600 Ω

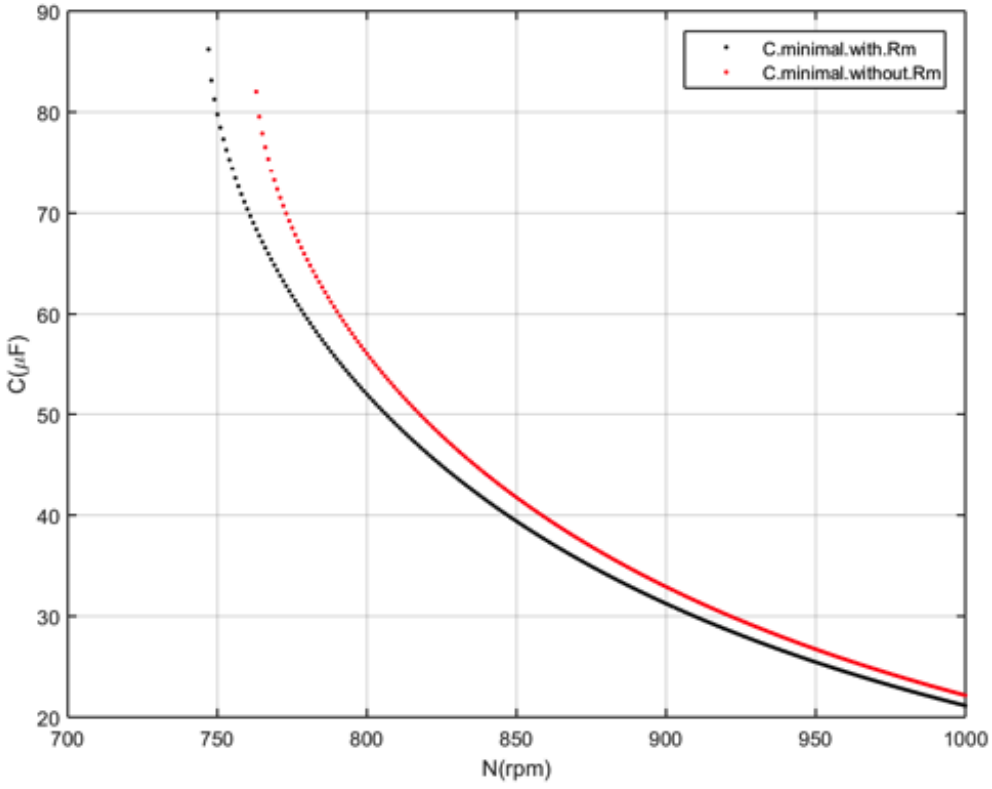

Figure 4-6. Required minimal capacitances for exciting a SEIG for R_L=300 Ω

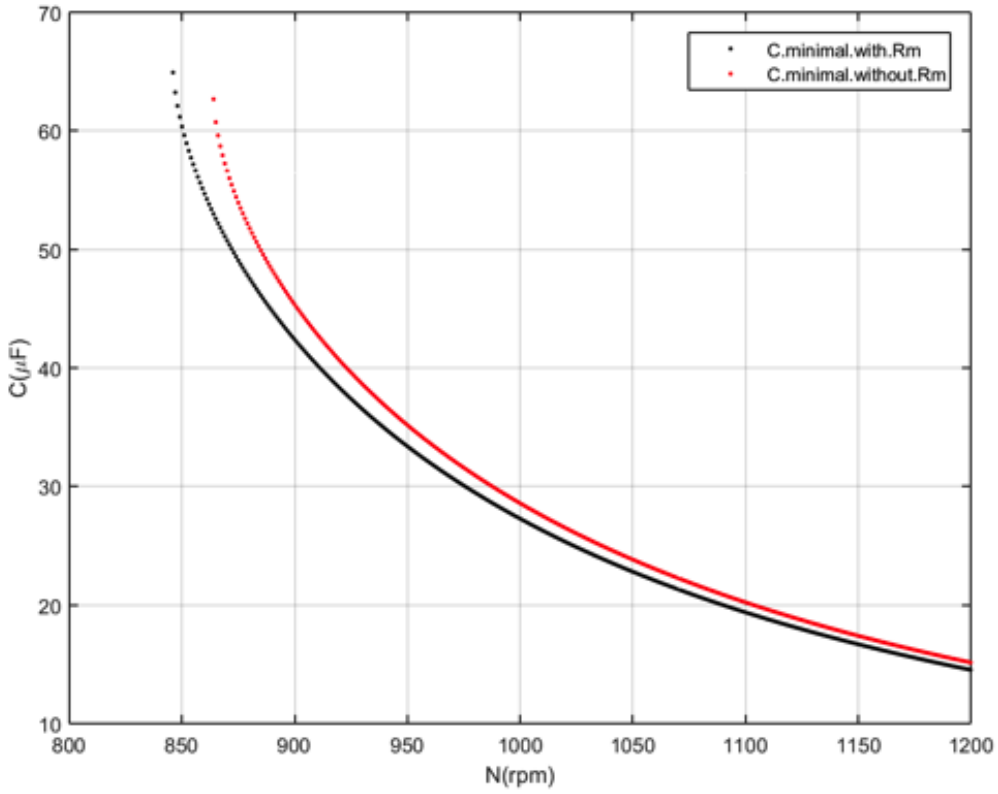

Figure 4-7. Required minimal capacitances for R_L= 230Ω

From the analysis of these results, it was possible to observe that, for a specific load, the capacitance value applied highly influences the rotational speed of the system. The capacitance required to keep the generator excited increased as the speed decreased. So, the lower the operational speed was, the higher the minimal capacitance was needed. The same occurred for the load variation.

From Figure 4-5, Figure 4-6 and Figure 4-7 it is seen that the minimal capacitances in the analytical model, where there was no regard towards the core losses, all the capacitors were over dimensioned. This is an important point to notice because every time there is an experimental work where the analytical model did not consider the core losses, it meant that for every speed the experimental work was made, the capacitance was overestimated, which might affect the longevity and well-functioning of the IG.

It is clearer when the speed is lower than the rated voltage the differences between models grew bigger. For $N < 800\, rpm$ the difference between both systems becomes higher, which can happen since for lower frequencies the effect of the magnetization is highlighted. This effect makes the induction generator to be easier to magnetize. So, the capacity for inducing some currents in the stators is facilitated. Hence, the SEIG does not need such Reactive Power to start operating.

4.3. Dynamics Analysis

In this section it is going to be simulated the SEIG machine with a creation of a proper Simulink simulation model which has the objective of recreating the environment of an Off-Grid SEIG scenario with the most possible accuracy.

4.3.1. Simulink Model

The purpose of this section is to explore the proper behavior of the whole system in off-grid scenario. For this approach, it must be considered all the research before mentioned in the chapter 3. It is necessary to create a SEIG machine for Simulink since the electrical library has an induction generator model that does not allow the user to set the electrical parameter variation, it only enables the user to set the electrical parameters as constant rated values. Hence, this Simulink induction generator is not useful for this work. So, to study all this operation conditions, it is needed to build a Simulink SEIG model that allows us to manipulate those parameters.

Before going into further detail, it is necessary to understand that for a 3-phase induction generator to be portrayed in Simulink is required to transform the machine from 3-phase to a 1-phase system, to simplify the calculations So, a Park transformation of the generator voltage and current where the phases $\begin{matrix} A \\ B \\ C \end{matrix}$ become $\begin{matrix} d \\ q \\ 0 \end{matrix}$ is required. After all the induction generator calculations are made, those currents and voltages must be transformed again from $\begin{matrix} d \\ q \\ 0 \end{matrix}$ into $\begin{matrix} A \\ B \\ C \end{matrix}$.

In Figure 4-8 it is shown the SEIG system composed of four blocks:

- Load
- Excitation
- Induction Generator
- Mechanical equation for determination of the speed of the machine.

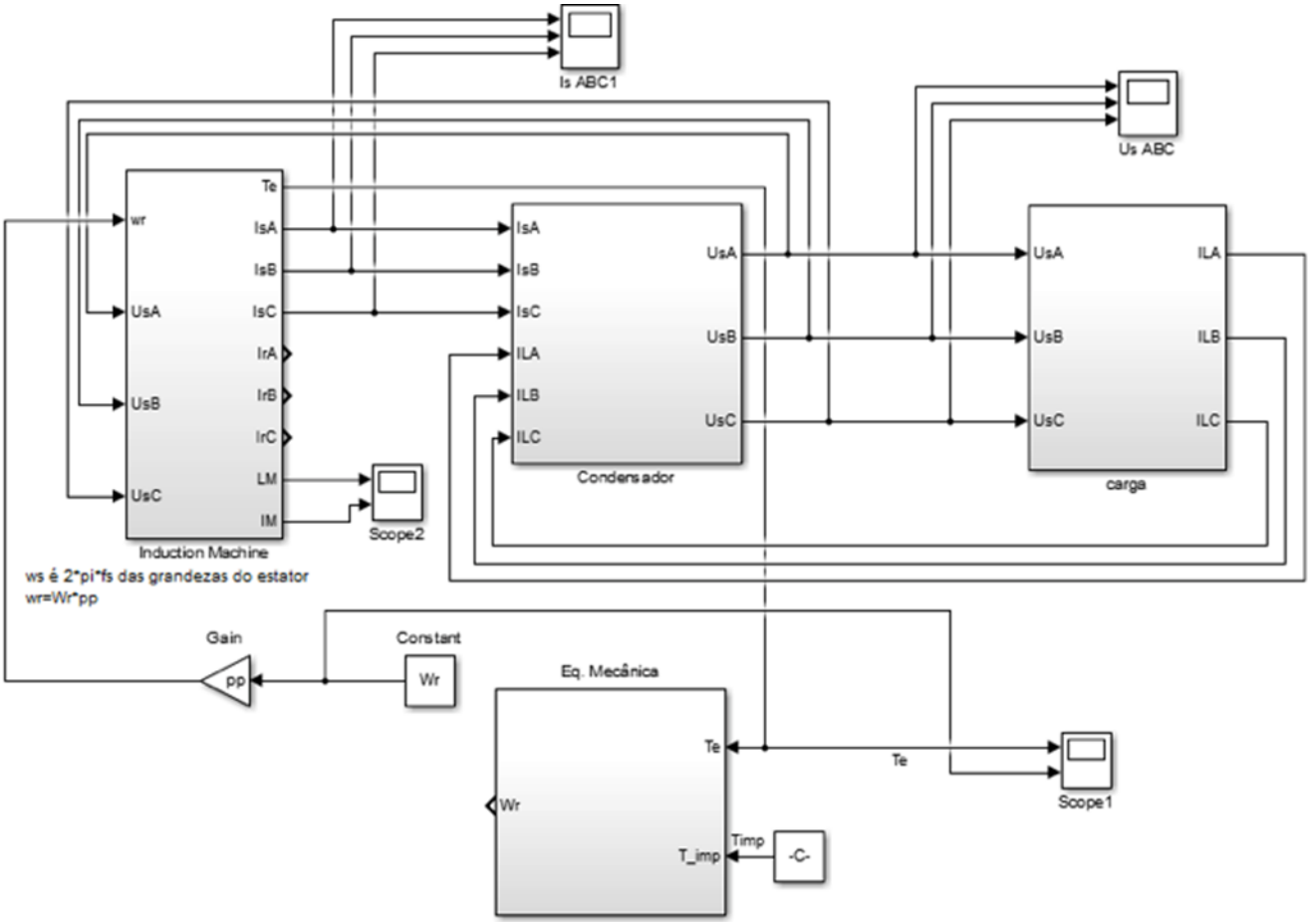

Figure 4-8. SEIG Simulink Model

The load block is modeled by the following equation (Kishore & Kumar, 2006)

$$i_{L_k} = \int \frac{1}{L} U_{s_k} - \frac{R}{L} i_{L_k}.\ k = A, B, C \tag{4.46}$$

From Figure 4-8 it is seen the three inputs of the load block, the three phases of the Stator voltages, as well as three outputs, the three phases of the load current. Figure 4-9 shows the load block developed in Simulink and three equations, $i_{L_A}, i_{L_B}, i_{L_C}$, that determine the load current.

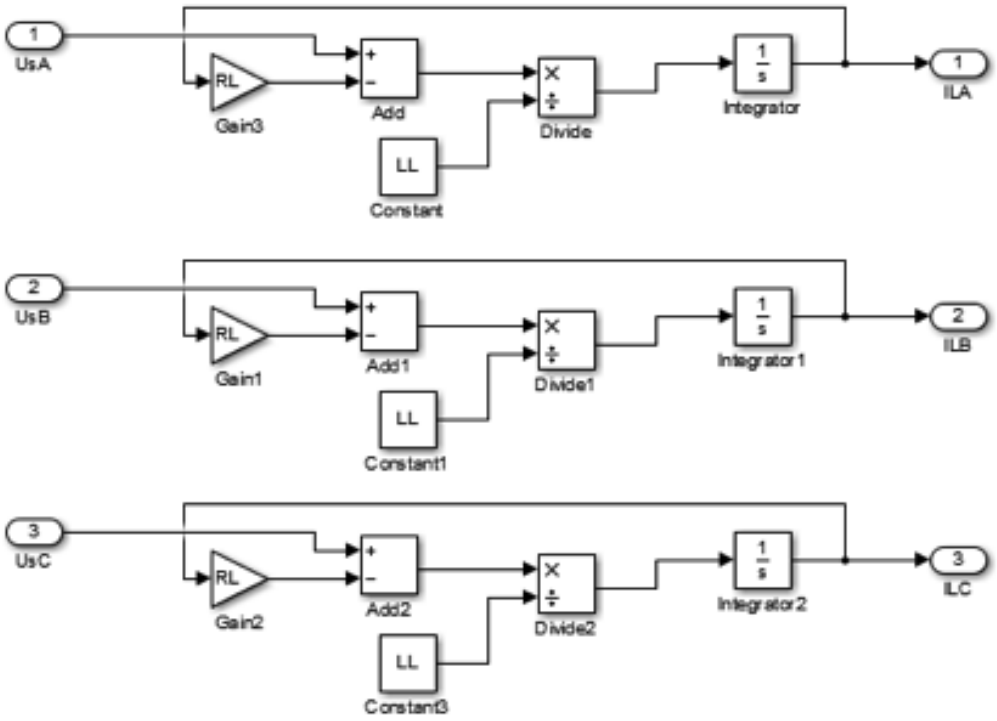

Figure 4-9. Load block for the SEIG Simulink Simulation

The excitation block, represented in Figure 4-10, is also a block with three equations, for each phase, where the inputs are the stator currents and the load currents that were developed in the load block. The outputs are the three phase stator voltages that goes into both load and induction generator blocks. These equations were presented by Kishore & Kumar (2006) during the work about a determination of a model of an off-grid SEIG using Space State approach.

$$U_{L_k} = \int \frac{1}{C} i_{s_k} - \frac{1}{C} i_{L_k}, \quad k = A, B. C \tag{4.47}$$

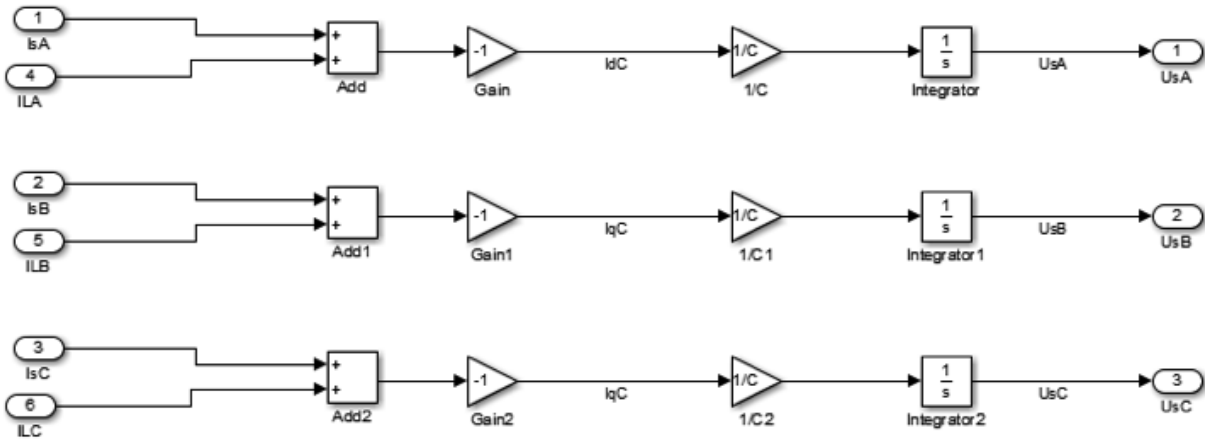

Figure 4-10. Excitation block for the SEIG Simulink Simulation

The mechanical equation block is where it is dictated the rotational speed at which the machine operates and is shown in equations (4.48) and (4.49). Equation (4.48) determines the electromagnetic torque, T_e, of the induction machine and equation (4.49) is the determination of the rotational speed of the SEIG:

$$T_e = \frac{3}{2} * \frac{pp}{2} * L_m(i_{d_s} \cdot i_{q_r} - i_{q_s} * i_{d_r}) \quad (4.48)$$

$$w_r = \int \frac{T_e - T_{imp}}{J} \quad (4.49)$$

In this work, it is important to notice that the imposed torque T_{imp} is the one that the PAT applies to SEIG system. For this imposed torque, it should be necessary to have a hydraulic study of the PAT, where the flow and head of the Water Transmission system should be studied in order to determine the mechanical equation for T_{imp} , in order to accurately portray the system (PAT-SEIG) in an off-grid scenario. Although it is an interesting topic of study, this is not one of the goals of this work and so, W_r is a constant value that must be manipulated by the user. This SEIG system portrays and emulates the experimental work where the SEIG was the only object of study.

The representation of the induction generator block can be found in Figure 4-11.

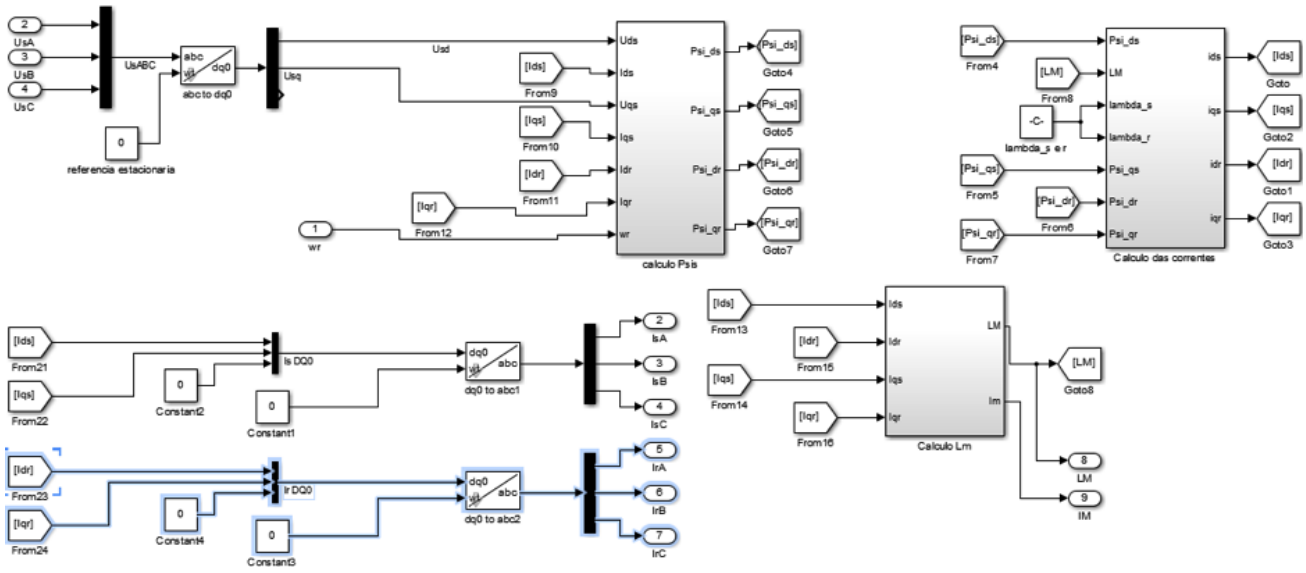

Figure 4-11. Induction generator block in the SEIG Simulink Model

The Simulink induction generator block represented in Figure 4-11 has 4 outputs, the 3 phases of the stator voltage and the rotational speed, and has 9 outputs, the 3 phases of the rotor and stator currents, the electromagnetic torque and both the magnetic induction and the magnetization current. First, it is necessary to have a Park Transformation to transform the induction generator into a one phase equivalent electric circuit. Then the computation for the magnetic flux and rotor and stator current are made. The principal of its computation follows these equations (Fernandes et al., 2018):

$$\psi_{d_s} = \int Ud_s - R_s i_{d_s} \quad (4.50)$$

$$\psi_{q_s} = \int Uq_s - R_s i_{q_s} \quad (4.51)$$

$$\psi_{d_r} = \int U_{d_r} - i_{d_r} * r_r + w_r * \psi_{q_r} \quad (4.52)$$

$$\psi_{q_r} = \int U_{q_r} - i_{q_r} * r_r + w_r * \psi_{d_r} \quad (4.53)$$

$$i_{d_s} = \frac{\psi_{d_s} - L_m * i_{d_r}}{L_s} \quad (4.54)$$

$$i_{q_s} = \frac{\psi_{q_s} - L_m * i_{q_r}}{L_s} \quad (4.55)$$

$$i_{d_r} = \frac{\psi_{d_r} - L_m * i_{d_s}}{L_r} \quad (4.56)$$

$$i_{q_r} = \frac{\psi_{q_r} - L_m * i_{q_s}}{L_r} \quad (4.57)$$

The final block before the inverse Park transformation, to transform the direct-quadrature (dq) variables into A, B, C variables it is the computation of the magnetic inductance. For the reasons above mentioned in the chapter 3, the only parameter that is going to be variable in this simulation is L_m and it was made with the help of many functions in Mat Lab called "*FlatTopLorentzian.m"*. What this function does is, using the L_m results in the no-load test of the chapter three, and determining the magnetizing current i_m, expressed in equation (4.58), it was able to create a graph that emulated the L_m behavior just as it was seen in chapter three in Figure 3-12. Figure 4-12 represents the graph created by the function that emulated L_m .

$$i_m = \sqrt{(i_{d_s} + i_{d_r})^2 + (i_{q_s} + i_{q_r})^2} \quad (4.58)$$

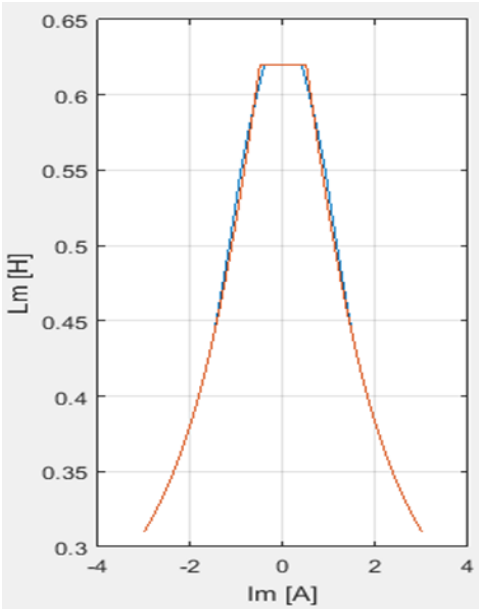

Figure 4-12. Graphic that illustrates how the function "FlatTopLorentzian.m" characterizes the inductive behavior of L_m

4.3.2. Simulation results

This simulation allows obtaining three different graphs:

- The three phases of the Stator voltage:
- The three phases of the Stator current;
- The electrical torque and the rotational speed of the machine;

To compare the values between the experimental capacitance values many simulations were performed. For three different purely resistive loads of 206, 411 and 714 ohms, the model was simulated for different speeds and different capacitances. For a defined speed, it would be necessary to run some more simulations until it was found the smallest capacity possible in order the machine to start and for the output of stator current reached its nominal value of 1.6A. Although it is not being compared the smallest capacity possible, the capacitance value that were taken into consideration are similar to those ones, sometimes the difference of some μF.

The figures below, Figure 4-13, Figure 4-14 and Figure 4-15, show the result of the simulations for a load value 206Ω. Figure 4-13 shows the behavior of the three phases of the stator voltage. This picture represents well the behavior of an SEIG because only after a few seconds it starts to operate at its rated values. Figure 4-14 is the behavior of the three phases of the stator current. Finally, Figure 4-15 shows the behavior of the torque in the SEIG. It is possible to see where the machine starts operating which is the point where the torque suffers a great increase until it stabilizes in 2.5 $(\frac{N}{m})$. This value corresponds to the torque rated value and it is obtained in the equation (4.59):

$$T_{e\,N} = \frac{P_N}{\frac{w_r * 2\pi * pp}{60}} \tag{4.59}$$

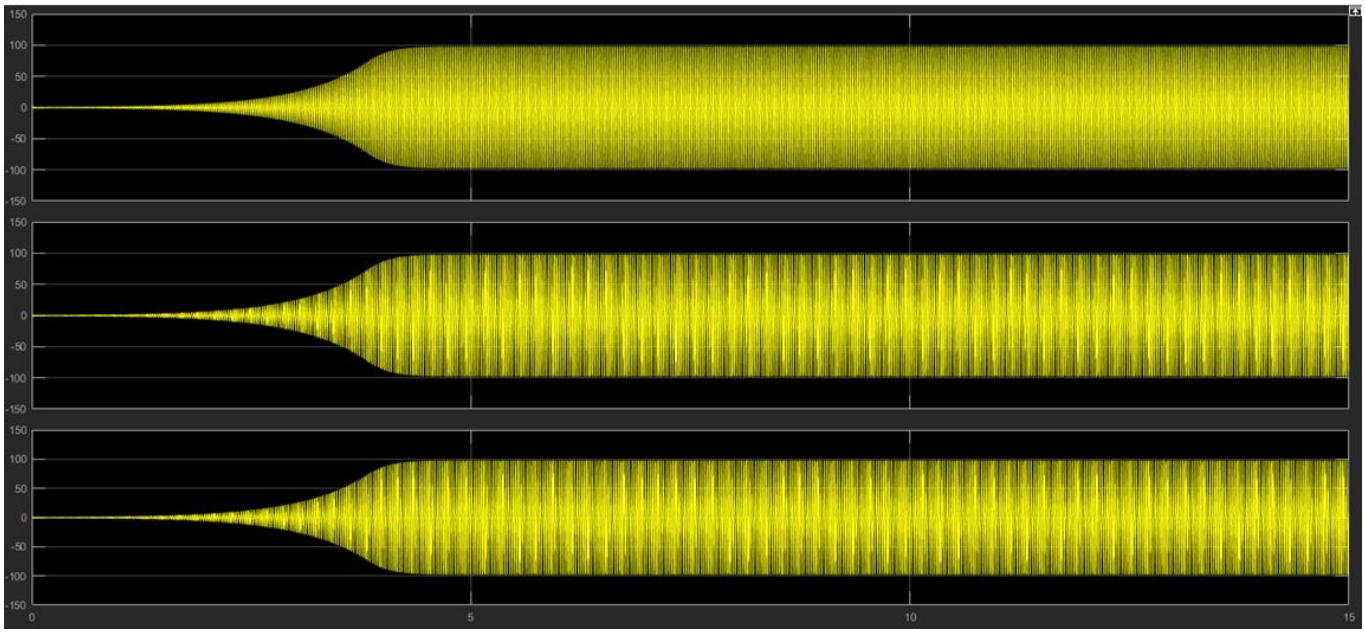

Figure 4-13. Stator voltage results for a resistance of $R = 206\,\Omega$ and an excitation of $C = 38\mu F$ and for a time range of 15 seconds.

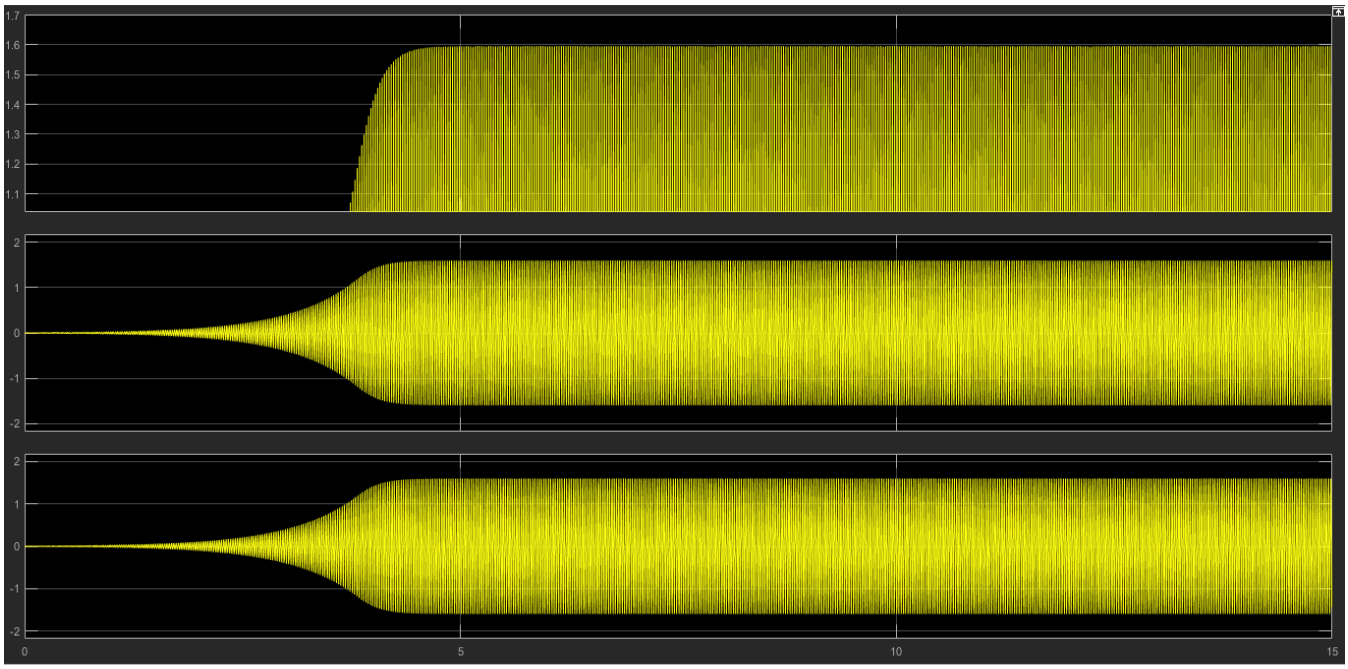

Figure 4-14. Stator current results for a resistance of $R = 206\Omega$ and an excitation of $C = 38\mu F$ and for a time range of 15 seconds

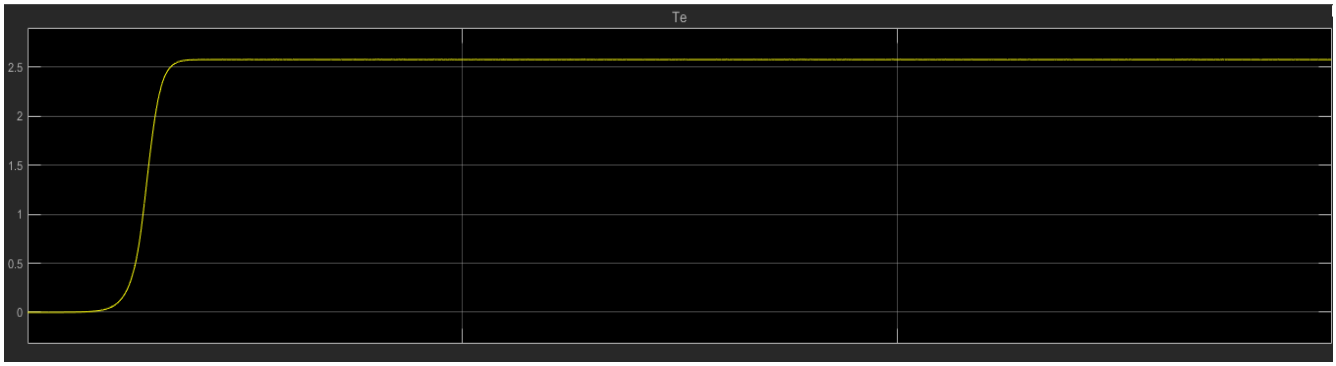

Figure 4-15. Electromagnetic Torque ($\frac{N}{m}$) result for a resistance of $R = 206\,\Omega$ and an excitation of $C = 38\mu F$ and for a time range of 15 second

4.4. Experimental Work

To analyze the behavior of the SEIG, an experimental system was assembled in the Electrical Machines Laboratory. The objective of these experimental tests was to analyze the performance of a SEIG and to determine the minimal required capacitance to make the SEIG work under nominal conditions. It is also considered a comparison between the determined capacitances in the simulation tests and the real capacitances, in order to validate the simulation model. Finally, it is also assessed the capacitor bank influence on the system.

The scheme of the experimental system is represented in Figure 4-16. In the assembled system, the prime mover chosen was a DC motor, connected to the SEIG in study.

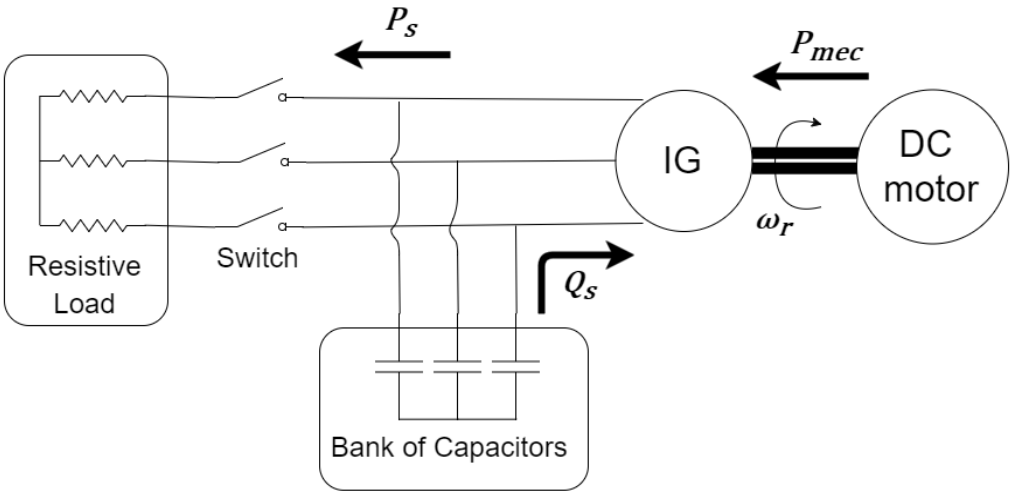

Figure 4-16. Scheme of the assembled experiment made in the Electrical Machines Lab

The nameplate of the Induction generator and the DC motor are shown in Table 3-1 and Table 3-6, respectively. The detailed information about some equipment can be seen in Appendix A. The load used in the experiments is a purely resistive load.

4.4.1 Tests and results

The flowchart of the Figure 4-17 shows the sequence of the tests performed. For a load value, it is applied a constant current I_f and voltage V_f in the DC motor field circuit. It was done with the help of the DC power source in the bench and a variable resistor, which regulated the necessary field current ($0.51\ A$). Then with the help of a three-phase autotransformer, that has the goal of regulating the 3-phase voltage that comes from the grid (230 V, 50Hz) in order to regulate the speed of the DC Motor-SEIG system.

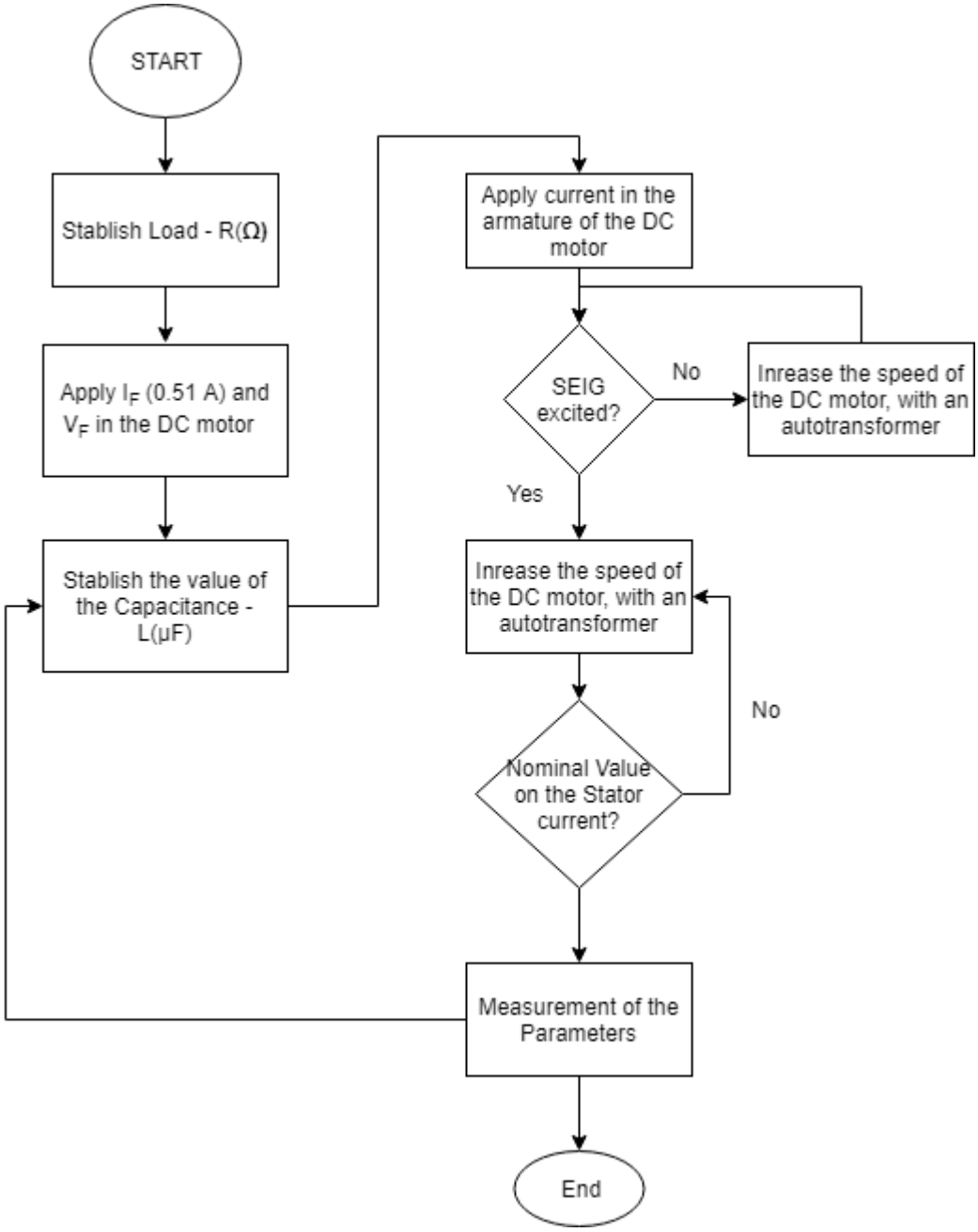

Figure 4-17. Flowchart of the experimental test in the DC-SEIG system

A diode rectifier is also necessary to convert the three-phase current to a monophasic current that feeds the armature of the DC Motor. Then, it is applied, in the system, the minimal capacitance that excites the generator. After it, the speed of the system keeps increasing until the machine gets excited and starts producing electrical power to feed the load, with recourse to the transformer. The final step of these tests is to increase the speed of the machine until the stator current in the generator reaches its nominal value of $1.6\,A$. Register all the measured values of the induction generator (the three phases of the stator voltages, V_s, the three phases of the stator current, I_s, the three phases of the active power, P_s, the three phases of the power factor, $\cos\varphi$) and the rotational speed of the whole system when the SEIG gets excited and when the generator stator current

reaches its nominal value. This process is repeated several times for different values of speed and capacitance.

There were some limitations throughout this experimental work. First, it was used two different machines. However, only one of the machines, referred in the chapter 3, was able to get excited for different levels of magnetization and for different speeds. The other machine could not be excited whatsoever. There was no level of capacitance or speed, which could excite that induction generator. The induction generator chosen for the experimental work had also a limitation because for every load value below $200\ \Omega$, and using all the possible combinations in the capacitor, the induction generator was unable to get excited and to produce any power to feed the load. To overcame this problems, it was necessary to replace the machine and the resistor.

Another limitation determined during the tests was that the capacitor bank was very limited and imprecise. It was two mechanical capacitor banks, linked in parallel, and each had two switches that were manipulated in order to get the desired level of magnetization. The problem was that one of the switches from one of the banks was not working properly, which limited the number of levels of capacitance that the system could work with. Even the combinations could not reach all the values of capacitance, which affects the system and the test results. As well as the capacitance, the load resistor suffered from the same problem. It was a variable mechanical resistor with two switches, one that reaches a higher specter of values and another one with a lower range but with a higher precision. There were made three tests with different values of the resistive load: $206\ \Omega$, $411\ \Omega$, $714\ \Omega$.

The results of the experiments for resistance $714\ \Omega$ are shown In Table 4-1, which can be seen two speeds, respectively: the minimal speed that allowed to excite the machine and the speed where the machine achieved its nominal values. For each value of the nominal value, for comparing the results with the simulation ones, it is registered the capacitance, the voltage, the current, the power the machine produces and its power factor.

Table 4-1. Experimental Results for a resistance of 714 ohms

			Voltage (V)			Current (A)			Power (kW)			Power Factor		
$N\ (rpm)$		$C(\mu F)$	U_1	U_2	U_3	I_1	I_2	I_3	P_1	P_2	P_3	pf_1	pf_2	pf_3
481	559	90	101.3	103	100.4	1.61	1.60	1.62	0.022	0.025	0.027	0.151	0.164	0.176
525	603	75	111.7	113.4	110.5	1.64	1.59	1.63	0.026	0.028	0.030	0.140	0.153	0.166
575	659	65	125.4	126.7	123.7	1.64	1.60	1.62	0.031	0.033	0.035	0.151	0.164	0.176

			Voltage (V)			Current (A)			Power (kW)			Power Factor		
$N\ (rpm)$		$C(\mu F)$	U_1	U_2	U_3	I_1	I_2	I_3	P_1	P_2	P_3	pf_1	pf_2	pf_3
661	743	45	141.6	144.1	140.4	1.58	1.55	1.59	0.037	0.041	0.043	0.166	0.182	0.190
690	793	40	153.3	155.6	151.0	1.60	1.60	1.61	0.042	0.047	0.047	0.173	0.189	0.193
802	888	35	174.1	178.3	173.0	1.56	1.51	1.56	0.052	0.059	0.061	0.192	0.210	0.216
849	923	30	182.1	183.1	177.8	1.62	1.66	1.60	0.058	0.082	0.063	0.194	0.268	0.220
845	938	30	171.5	172.8	177.4	1.56	1.50	1.57	0.072	0.064	0.066	0.190	0.236	0.238
884	970	30	190.9	195.1	188.6	1.59	1.59	1.60	0.064	0.069	0.070	0.208	0.223	0.231
950	992	30	193.6	199	192.6	1.64	1.59	1.66	0.042	0.047	0.047	0.208	0.226	0.229
1001	1107	25	218.5	223.0	214.9	1.61	1.60	1.60	0.064	0.069	0.070	0.208	0.223	0.231
1061	1122	20	222.1	222.9	215.5	1.62	1.68	1.60	0.036	0.037	0.034	0.228	0.324	0.258
1020	1126	20	220.0	221.2	213.2	1.60	1.66	1.57	0.082	0.119	0.087	0.230	0.323	0.259
1109	1161	20	207.2	208.2	217.0	1.61	1.60	1.61	0.081	0.094	0.087	0.228	0.264	0.216
1142	1224	16	240.3	246.7	237	1.60	1.59	1.60	0.097	0.105	0.105	0.253	0.259	0.278

The experimental results for $206\ \Omega$ and $411\ \Omega$ can be seen in Annex F.

4.4.2 Comparison between Simulation and Experimental Results

For the comparison of both experimental and simulation values, the figures below show two curves. One with points, which represents all the experimental points measured for a given load. From these points, it was made an interpolation, which can be observed as the striped curve in Figure 4-18 to Figure 4-20, and then they were compared with the simulation values from this work, which is the interpolated curve without marks.

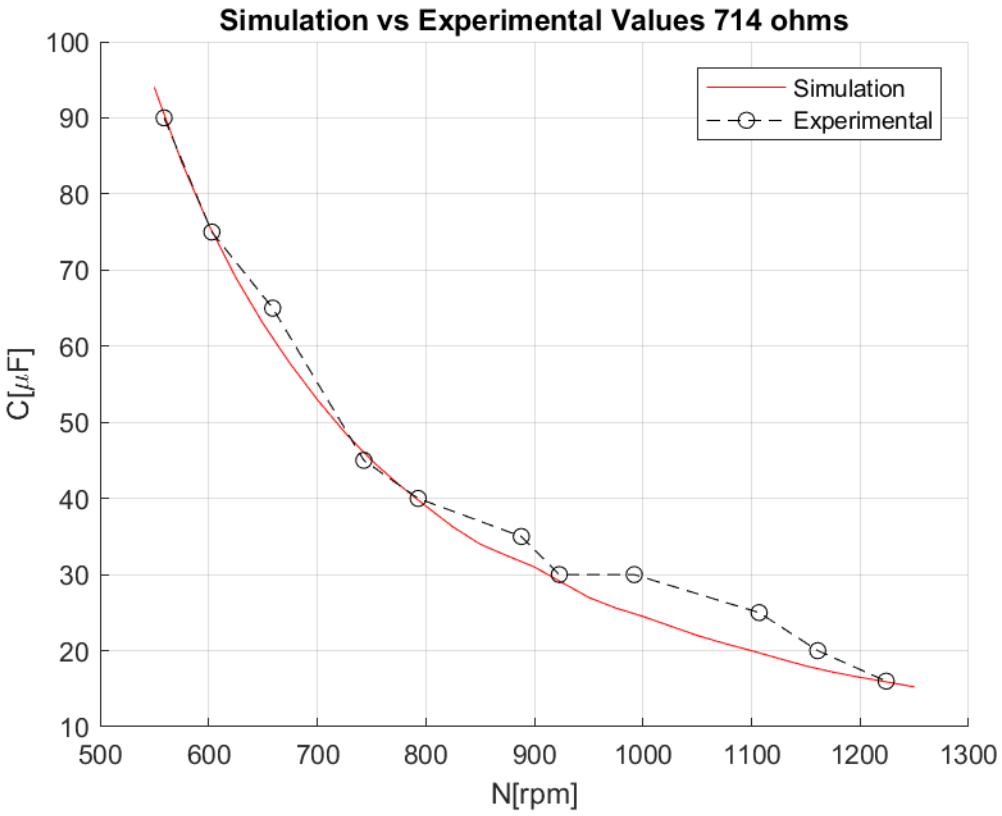

Figure 4-18. Comparison between experimental and simulation values for $R = 714\ \Omega$

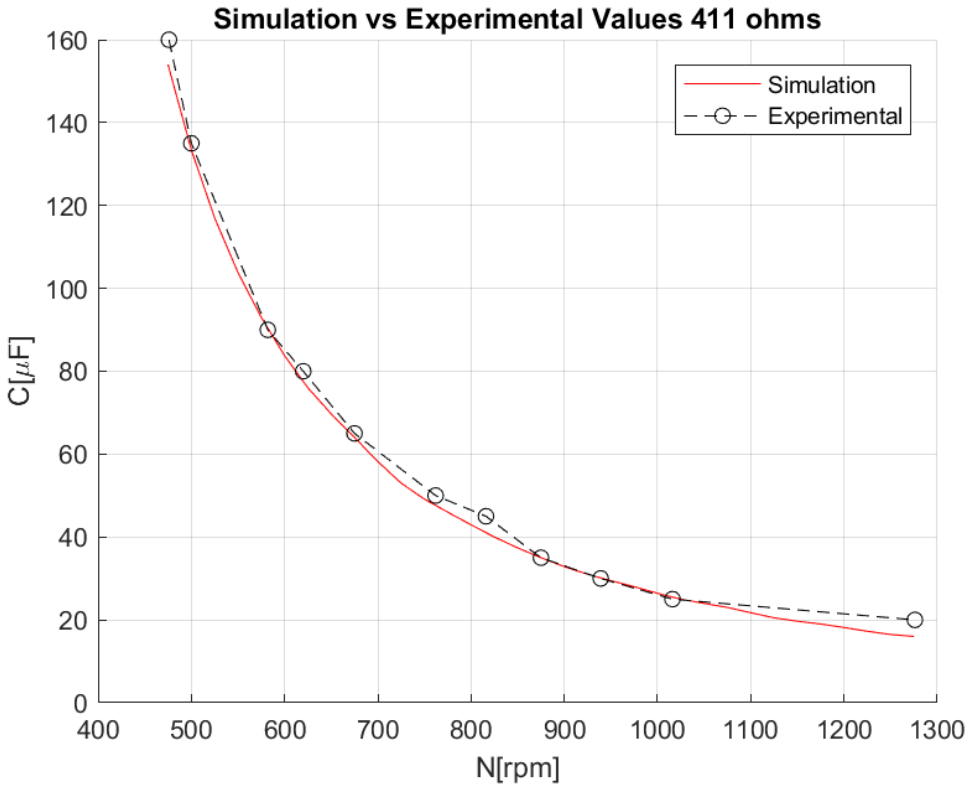

Figure 4-19. Comparison between experimental and simulation values for $R = 411\Omega$

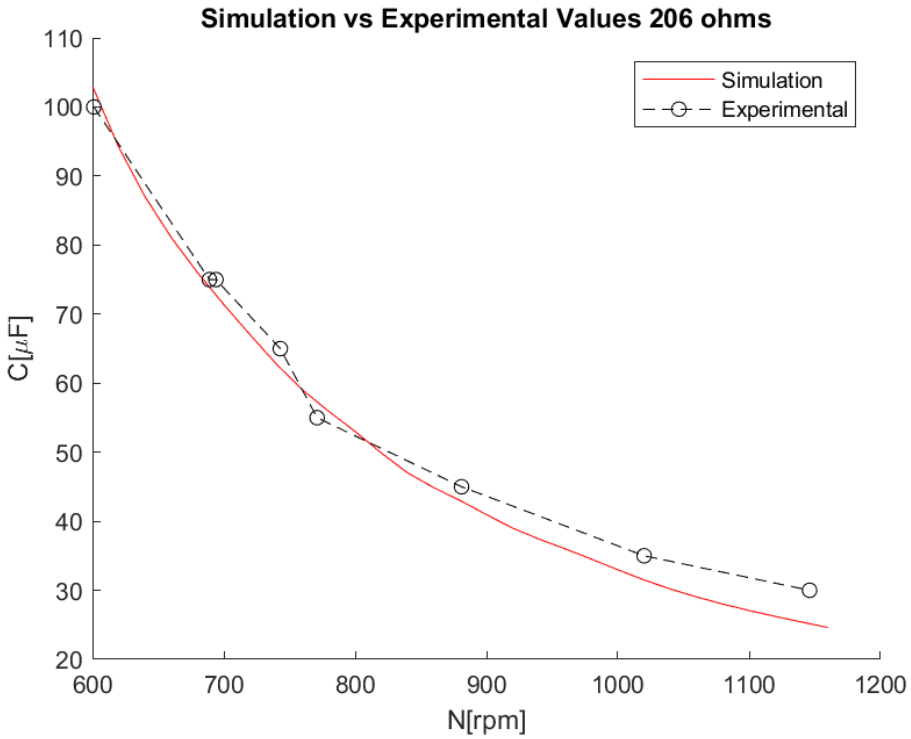

Figure 4-20. Comparison between experimental and simulation values for $R = 206\,\Omega$

From these results, the validation of the model was achieved due to the similarity between the results obtained by the simulation and obtained from experimental work. By looking at these results it is clear to see that this SEIG model has a better performance for higher resistances. In all three cases it is shown that, once again, the speed of the generator is highly influenced by its excitation, which it depends on the load. For higher values of load resistance, the capacitance required presented smaller variations for the same speed.

Concluding, this simulation method presented small differences of results with the experimental case and the general behavior of the SEIG was equal on all simulations performed. The simulation performed here shows that the work of a SEIG presents considerable limitations and is highly influenced by the bank capacitance and load values, as expected.

4.5. Chapter Conclusion

The work performed in this chapter had the purpose of analyzing the operation and performance of a SEIG, further to be applied in a PAT system. To estimate and understand the range of the needed bank of capacitors, two models were developed. First, an analytical model was developed, allowing the computation of the minimal range of capacitances, for a given load. Then, for the estimated values, a simulation model was developed, to analyze the behavior of the SEIG operation. These two models allowed a complete estimation of the SEIG performance, being compared with the experimental values determined in the laboratory

As shown in section 4.2.2, Results for the Analytical Model, the magnetization parameters are in fact relevant for a construction of an analytical and simulation model. From experimental tests, it was verified that Rr, Rm, and Lm, had a high oscillation for different speeds and loads. Both Rm and Lm parameters mainly depend on the magnetic flux (E/f (magnetization voltage/electrical frequency)). The Lm parameter had a high impact in the model accuracy due to its dependence on the magnetic flux, while the variation of the remaining parameters is almost insignificant. Related to this analysis, the impact of choosing the wrong capacitor values can cause the overload of the SEIG or the non-excitation of it. This overload can be problematic for the machine because it is believed that the machine is operating in a certain speed and in reality, the machine is running in a higher speed. It can cause the machine to work in speeds and currents higher than the nominal ones, which, over time, might result in the machine decay. This is important, since these values are significant when we are in a situation where both frequency and voltage are not regulated, since they depend on the flow and head in the water systems, which is dependent upon the load. Hence, the PAT+SEIG system has to be adjusted to the rotational speed continuously, in order to maximize the recovered energy.

As shown in section 4.4.2, analysis of the simulation results, the estimated performances did not differ considerably from the experimental case. Therefore, the simulation in Simulink is a reliable source for estimating the range of capacitances.

To sum up, the development of this methodology has a great impact in the accuracy for the modeling of the SEIG and it must be made into account for future researches in SEIG working in an off-grid conditions. For a future research it is suggested to study the overall efficiency of the SEIG machine in order to maximize the capacity of recovering energy and in order to determine the best induction machine for operating in off-grid.

5. Conclusions and recommendations for future studies

The study of the application of system SEIG + PAT has increased over the years, as it was discovered the PAT is a considerably cheaper alternative for recovering energy. Electrical and Hydraulic regulation modes are the two designs which were given the biggest study throughout the years, both of them applied in a system connected to the electrical grid.

In this work, one analyzed the off-grid approach. It is a study of great interest for applications in countries where the national electrical grid is underdeveloped as this can be cheaper and a more reliable source of energy for populations with fewer possibilities. This work was intended to analyze a 500 Watts SEIG system, further to be applied in a PAT. This work was divided into two parts: Study the behavior of the induction generator parameters with frequency and voltage and a SEIG analysis.

Concerning the behavior of the induction generator, the research establishes the influence of the capacitor values to SEIG on the overall system operation points regarding non-normal conditions which is non-regulated voltage and frequency. From previous studies, the lack of accuracy of analytical models based on electrical equivalent circuit of the SEIG was verified when considering fixed electrical parameters and neglecting the iron losses or the magnetic inductance. This analysis demonstrated that it is important to develop more accurate analytical models when the pumps working as turbines are installed in water systems and they are off-grid.

Regarding the SEIG analysis, this thesis showed better results from previous studies when the variation of the SEIG electrical parameters were not considered as a function of the electrical frequency and applied voltage and also when the iron losses were not considered in the model. For this analysis to occur an analytical and simulation model were made with the attention of non-fixed parameters of the induction generator. From experimental tests, all the parameters had high changes for different speed and loads. Both R_m and L_m parameters mainly depend on the magnetic flux. It was demonstrated that with this new approach, both analytical and simulation model have a better accuracy when compared with the experimental results.

From a general perspective, the application of this isolated SEIG+PAT system can be an interesting solution for combining the pressure reduction in WDS with energy generation. With this new study, the performance of SEIG+PAT could be highly improved. It can be achieved with the presence of a bank of capacitors that allows to change the rotational speed and adapt it to the working conditions at each moment.

The use of this methodology will allow water managers to choose the hydraulic machine as a function of not only the hydraulic characteristic but also the electric machine (PAT + SEIG) that considers the available recovery points.

From the work performed here, some problems were observed. This thesis required bigger investment in experimental work, such as the whole efficiency study of the machine and the application from the SEIG+PAT system in a hydraulic laboratory. In addition, and for future references, while doing a similar work there is the need to find a machine that works better under off-grid scenarios. There were some situations where the machine simply did not operate for some speeds that were supposed to operate. Finally, it is required for a development of a controlling system, depending on the working conditions, that could be able to control the frequency in an off-grid scenario. In order to have better efficiency, the controllers could regulate and control the frequency and/or the stator voltage. With this, it is expected that the total efficiency of the system (PAT + SEIG) would be improved.

So, the future work related to this project can be summarized by the following topics:

- Complete study of the efficiency study of the SEIG+PAT system
- Develop controlling electronic system to maximize the operation of the PAT, by controlling the electrical frequency of the machine;
- Switch the mechanical bank of capacitors with an electrical one, which enable the user of a wider range and precision in the value of the capacitance, for further studies and for a better efficiency of the system, and
- Connect the system to a battery to study the SOC of the battery and to test if this system is effective in the battery recharge process.

6. Bibliography

Abbou, A., Barara, M., Ouchatti, A., Akherraz, M., & Mahmoudi, H. (2013). Capacitance required analysis for self-excited induction generateur. *Journal of Theoretical and Applied Information Technology*, *55*(3), 382–389.

Buono, D., Frosina, E., Mazzone, A., & Cesaro, U. (2015). *Study of a Pump as Turbine For a Hydraulic Urban Network Using a Tridimensional CFD Modeling Methodology*. *82*, 201–208. https://doi.org/10.1016/j.egypro.2015.12.020

Capelo, B. (2017). *Energy Recovery in Water Distribution Systems by a Pump Running as Turbine (PAT) – Grid Isolated Case*. Instituto Superior Técnico, Universidade de Lisboa.

Capelo, B., Pérez-sánchez, M., Fernandes, J. F. P., Ramos, H. M., López-jiménez, P. A., & Branco, P. J. C. (2017). Electrical behaviour of the pump working as turbine in off grid operation. *Applied Energy*, (September), 0–1. https://doi.org/10.1016/j.apenergy.2017.10.039

Chan, T. F. (1993). Capacitance requirements of self-excited induction generators. *IEEE Transactions on Energy Conversion*, *8*(2), 304–311. https://doi.org/10.1109/60.222721

Dente, A. (2007a). *Elementos de Electrotecnia - Capítulo: Máquina Assíncrona*.

Dente, A. (2007b). *Elementos de Electrotecnia - Capítulo: Máquina de Corrente Contínua*.

Dente, A. (2007c). *Elementos de Eletrotecnia - Capítulo: Circuito Magnético*.

Eltamaly, A. M. (2002). *New Formula to Determine the Minimum Capacitance Required for Self-Excited Induction Generator*. Elminia University, Elminia, Egypt.

Fernandes, J. F. P., Pérez-sánchez, M., Silva, F. F., López-jiménez, P. A., Ramos, H. M., & Branco, P. J. C. (2018). *Optimal Energy Efficiency of Isolated PAT systems by SEIG Excitation Tuning*. 1–26.

Giraud, F., & Salameh, Z. M. (1998). Wind-driven, variable-speed, variable-frequency, double-output, induction generators. *Electric Machines and Power Systems*, *26*(3), 287–297. https://doi.org/10.1080/07313569808955823

Kishore, A., & Kumar, G. S. (2006). Dynamic modeling and analysis of three phase self-excited induction generator using generalized state-space approach. *International Symposium on Power Electronics, Electrical Drives, Automation and Motion,* 1459–1466.

Kumawat, R. K., Chourasiya, S., Agrawal, S., & Paliwalia, D. K. (2015). Self excited induction generator: A review. *International Advanced Research Journal in Science, Engineering and Technology (IARJSET)*, *2*(1). https://doi.org/10.17148/IARJSET

Paiva, J. P. S. (2011). *Redes de Energia Elétrica - Uma análise sistemática* (3ª). IST Press.

Pena, R. S., Asher, G. ., Clare, J. C., & Cardenas, R. (1996). A constant frequency constant voltage variable speed stand alone wound rotor induction generator. *Opportunities and Avances in International Power Generation*, (419), 111–114. https://doi.org/10.1049/cp:19960129

Raina, G., & Malik, O. P. (1983). Wind energy conversion using a self-excited induction generator. *IEEE Transactions on Power Apparatus and Systems*, *PAS-102*(12), 3933–3936. https://doi.org/10.1109/TPAS.1983.317933

Ramos, H., & Borga, A. (2000). *Pumps as turbines : an unconventional solution to energy production*. *1*(1999), 261–263.

Samora, I., Franca, M. J., Schleiss, A. J., & Ramos, H. M. (2016). Simulated Annealing in Optimization of Energy Production in a Water Supply Network. *Water Resources Management*, *30*(4), 1533–1547. https://doi.org/10.1007/s11269-016-1238-5

Singh, B., Singh, M., & Tandon, A. K. (2010). Transient Performance of Series-Compensated Feeding Dynamic Loads. *IEEE Transactions on Industry Applications*, *46*(4), 1271–1280.

Valadão, R. (2012). *Análise do comportamento de um gerador de indução trifásico autoexcitado por capacitores*. Universidade Federal do Rio de Janeiro.

Wright, R., Abraham, E., Parpas, P., & Stoianov, I. (2015). Optimized control of pressure reducing valves in water distribution networks with dynamic topology. *Procedia Engineering*, *119*, 1003–1011. https://doi.org/10.1016/j.proeng.2015.08.994

Xu, K., Xie, N., Wang, C., & Shi, X. (2017). Modeling and Simulation of Variable Speed Variable Frequency Electrical Power System in More Electric Aircraft. *The Open Electrical & Electronic Engineering Journal*, *11*(1), 87–98. https://doi.org/10.2174/1874129001711010087

Apendix

Annex A. Equipment used in experimental aplictions

- **Power Logger Fluke 1735**

Model: Fluke 1735 three-phase power logger

Memory: 4MB flash memory – 3.5MB for measuring data

Sample Rate: 10.24 kHz

V-RMS wye resolution: 0.1V

Operating Error: ±0.5% of measured value +10 digit

A-RMS resolution: 0.01 A

- **Tektronik TDS 2001/2012C Oscilloscope**

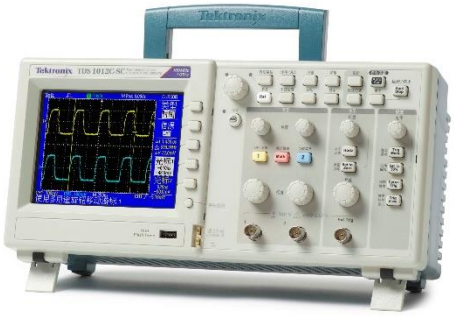

Brand. Tektronix

Model: TDS 2001/2012C

Analog Bandwith: 100MHz

Sample Rate: 2 GS/s

Record: 2.5k Point

Analog Channels: 2

- **Capacitor banks Esselte Studium**

Brand: ESSELTE STUDIUM

Power: 3.2 kVAr

Frequency: 50 Hz

Maximum capacitance: 3·60 µF

Connections:

Δ - 3·220 V ; 1.2 - 8.4 A

Y - 3·380 V ; 0.7 – 4.9 A

/// - 220V ; 2.1 – 14.5 A

Annex B: Results of the no-load test

- f = 30 Hz

$Uc\ [V]$	80	100	120	140	160	180	190	200
$U_1\ [V]$	*47*	*57,6*	*69,2*	*80,9*	*92,6*	*104,8*	*109,5*	*114,5*
$U_2\ [V]$	*46,9*	*57,5*	*69*	*81,1*	*92,9*	*104,2*	*109,4*	*114,2*
$U_3\ [V]$	*46,9*	*57,6*	*69,2*	*81,1*	*92,8*	*104,4*	*109,4*	*114*
$I_1\ [A]$	*0,36*	*0,45*	*0,54*	*0,65*	*0,77*	*0,89*	*0,95*	*1,01*
$I_2\ [A]$	*0,37*	*0,46*	*0,55*	*0,66*	*0,77*	*0,9*	*0,96*	*1,02*
$I_3\ [A]$	*0,36*	*0,45*	*0,54*	*0,65*	*0,76*	*0,89*	*0,95*	*1,01*
$P_1\ [kW]$	*0,006*	*0,008*	*0,01*	*0,014*	*0,018*	*0,023*	*0,026*	*0,029*
$P_2\ [kW]$	*0,006*	*0,008*	*0,01*	*0,014*	*0,018*	*0,023*	*0,026*	*0,029*
$P_3\ [kW]$	*0,006*	*0,008*	*0,011*	*0,014*	*0,019*	*0,024*	*0,027*	*0,03*
$Q_1\ [kVAr]$	*0,017*	*0,026*	*0,037*	*0,053*	*0,071*	*0,093*	*0,105*	*0,115*
$Q_2\ [kVAr]$	*0,017*	*0,026*	*0,038*	*0,053*	*0,072*	*0,094*	*0,105*	*0,116*
$Q_3\ [kVAr]$	*0,017*	*0,026*	*0,037*	*0,052*	*0,071*	*0,093*	*0,104*	*0,115*
p_{f_1}	*0,342*	*0,305*	*0,273*	*0,259*	*0,253*	*0,247*	*0,25*	*0,25*
p_{f_2}	*0,337*	*0,301*	*0,269*	*0,254*	*0,249*	*0,247*	*0,246*	*0,245*
p_{f_3}	*0,355*	*0,313*	*0,285*	*0,273*	*0,261*	*0,258*	*0,26*	*0,26*
$N\ [rpm]$	*595*	*595*	*604*	*602*	*603*	*603*	*599*	*601*

- f = 40 Hz

$Uc\ [V]$	105	130	160	190	210	240	250	260
$U_1\ [V]$	61	75,5	92,3	108,5	121,8	137,8	145	152,1
$U_2\ [V]$	61	75,5	92,5	108,5	122	137,8	145	152
$U_3\ [V]$	61	75,4	92,6	108,6	121,7	137,9	144,6	151,9
$I_1\ [A]$	0,36	0,45	0,56	0,67	0,76	0,9	0,96	1,02
$I_2\ [A]$	0,36	0,45	0,56	0,68	0,77	0,91	0,96	1,03
$I_3\ [A]$	0,36	0,45	0,56	0,67	0,76	0,9	0,96	1,02
$P_1\ [kW]$	0,007	0,009	0,012	0,017	0,02	0,026	0,029	0,033
$P_2\ [kW]$	0,007	0,009	0,013	0,017	0,02	0,027	0,029	0,033
$P_3\ [kW]$	0,008	0,01	0,013	0,018	0,022	0,028	0,031	0,035
$Q_1\ [kVAr]$	0,022	0,034	0,051	0,074	0,093	0,124	0,138	0,156
$Q_2\ [kVAr]$	0,022	0,034	0,052	0,075	0,093	0,125	0,139	0,157
$Q_3\ [kVAr]$	0,022	0,034	0,051	0,074	0,092	0,124	0,138	0,156
p_{f_1}	0,324	0,26	0,24	0,223	0,216	0,212	0,212	0,212
p_{f_2}	0,322	0,269	0,244	0,226	0,218	0,213	0,211	0,212
p_{f_3}	0,339	0,285	0,26	0,242	0,234	0,228	0,226	0,224
$N\ [rpm]$	796	800	800	798	801	798	802	793

- f = 50 Hz

$Uc\ [V]$	50	100	150	200	250	300	350	400
$U_1\ [V]$	28,7	57,7	86,4	116	143,7	172,8	201,6	230,5
$U_2\ [V]$	29	58,1	87	116,3	144,2	173,4	203	231,9
$U_3\ [V]$	28,7	58,3	86,6	115,9	144,5	173,8	204,2	233,1
$I_1\ [A]$	0,19	0,27	0,4	0,55	0,71	0,9	1,13	1,47
$I_2\ [A]$	0,19	0,28	0,41	0,56	0,72	0,91	1,17	1,5
$I_3\ [A]$	0,19	0,29	0,42	0,57	0,74	0,92	1,17	1,52
$P_1\ [kW]$	0,004	0,006	0,01	0,015	0,021	0,031	0,044	0,071
$P_2\ [kW]$	0,004	0,006	0,01	0,014	0,019	0,029	0,041	0,063
$P_3\ [kW]$	0,004	0,006	0,01	0,015	0,023	0,031	0,049	0,074
$Q_1\ [kVAr]$	0,005	0,016	0,035	0,064	0,1	0,156	0,227	0,343
$Q_2\ [kVAr]$	0,005	0,016	0,035	0,064	0,104	0,159	0,237	0,348
$Q_3\ [kVAr]$	0,005	0,017	0,035	0,066	0,107	0,16	0,239	0,357
p_{f_1}	0,733	0,374	0,278	0,232	0,216	0,199	0,193	0,207
p_{f_2}	0,733	0,35	0,241	0,213	0,181	0,182	0,173	0,181
p_{f_3}	0,692	0,347	0,27	0,218	0,212	0,195	0,203	0,205
$N\ [rpm]$	924,5	980	983	989	992,2	994	995,3	995,3

- f = 60 Khz

$Uc\ [V]$	157	200	250	300	350	387	387	387
$U_1\ [V]$	91	115,9	145	172,9	203,7	223,7	223,7	223,7
$U_2\ [V]$	91	115,8	145	172,7	203,5	224	224	224
$U_3\ [V]$	90,9	115,9	145	172,8	203,6	224	224	224
$I_1\ [A]$	0,36	0,46	0,59	0,72	0,89	1,02	1,02	1,02
$I_2\ [A]$	0,37	0,47	0,59	0,73	0,89	1,02	1,02	1,02
$I_3\ [A]$	0,36	0,46	0,59	0,72	0,89	1,02	1,02	1,02
$P_1\ [kW]$	0,009	0,012	0,017	0,023	0,032	0,04	0,04	0,04
$P_2\ [kW]$	0,009	0,012	0,017	0,024	0,032	0,04	0,04	0,04
$P_3\ [kW]$	0,009	0,013	0,018	0,025	0,035	0,042	0,042	0,042
$Q_1\ [kVAr]$	0,033	0,054	0,085	0,124	0,18	0,227	0,227	0,227
$Q_2\ [kVAr]$	0,033	0,054	0,086	0,125	0,182	0,229	0,229	0,229
$Q_3\ [kVAr]$	0,033	0,054	0,086	0,124	0,181	0,228	0,228	0,228
p_{f_1}	0,267	0,222	0,201	0,184	0,177	0,174	0,174	0,174
p_{f_2}	0,275	0,228	0,203	0,188	0,176	0,175	0,175	0,175
p_{f_3}	0,295	0,242	0,215	0,201	0,191	0,186	0,186	0,186
$N\ [rpm]$	1184	1195	1198	1200	1196	1194	1194	1194

Annex C: Results for blocked rotor test

- f = 30 Hz

$I\ [A]$	0,7	0,8	0,9	1	1,2	1,35	1,5	1,6
$U_1\ [V]$	26,8	33,4	36,5	42,3	48,5	52,7	59,2	59,9
$U_2\ [V]$	26,6	33,1	36,2	41,9	48,3	52,6	58,6	59,4
$U_3\ [V]$	26,5	33,1	36,1	42,1	48,3	52,5	58,6	59,4
$I_1\ [A]$	0,68	0,82	0,9	1,05	1,22	1,33	1,5	1,55
$I_2\ [A]$	0,67	0,82	0,89	1,04	1,21	1,32	1,49	1,53
$I_3\ [A]$	0,69	0,84	0,91	1,07	1,23	1,34	1,52	1,56
$P_1\ [kW]$	0,015	0,023	0,027	0,037	0,05	0,059	0,075	0,078
$P_2\ [kW]$	0,014	0,022	0,026	0,036	0,048	0,058	0,073	0,076
$P_3\ [kW]$	0,015	0,023	0,027	0,037	0,05	0,059	0,075	0,078
$Q_1\ [kVAr]$	0,018	0,027	0,032	0,044	0,059	0,07	0,089	0,093
$Q_2\ [kVAr]$	0,018	0,027	0,032	0,044	0,058	0,069	0,087	0,092
$Q_3\ [kVAr]$	0,018	0,028	0,033	0,045	0,06	0,071	0,089	0,093
p_{f_1}	0,829	0,848	0,845	0,847	0,844	0,846	0,845	0,841
p_{f_2}	0,798	0,821	0,815	0,824	0,829	0,832	0,835	0,826
p_{f_3}	0,818	0,83	0,83	0,829	0,835	0,839	0,84	0,838
$N\ [rpm]$	0	0	0	0	0	0	0	0

- f = 40 Hz

$I\ [A]$	0,7	0,8	0,9	1	1,2	1,35	1,5	1,6
$U_1\ [V]$	31,7	37,4	42	46,6	54,6	60,9	67,8	69,9
$U_2\ [V]$	31,4	37,1	41,7	46,3	54,2	60,5	67,5	69,5
$U_3\ [V]$	31,3	37	41,6	46,1	54,2	60,5	67,5	69,4
$I_1\ [A]$	0,7	0,81	0,91	1,01	1,19	1,34	1,5	1,57
$I_2\ [A]$	0,68	0,79	0,89	0,99	1,18	1,32	1,49	1,55
$I_3\ [A]$	0,71	0,82	0,92	1,02	1,21	1,35	1,52	1,59
$P_1\ [kW]$	0,018	0,024	0,031	0,038	0,052	0,065	0,082	0,088
$P_2\ [kW]$	0,016	0,023	0,029	0,036	0,05	0,063	0,079	0,085
$P_3\ [kW]$	0,017	0,023	0,03	0,037	0,051	0,065	0,081	0,087
$Q_1\ [kVAr]$	0,022	0,03	0,038	0,047	0,065	0,081	0,102	0,11
$Q_2\ [kVAr]$	0,021	0,029	0,037	0,046	0,064	0,08	0,1	0,109
$Q_3\ [kVAr]$	0,022	0,03	0,038	0,047	0,065	0,082	0,102	0,111
p_{f_1}	0,792	0,8	0,807	0,805	0,8	0,804	0,801	0,799
p_{f_2}	0,759	0,773	0,776	0,77	0,779	0,785	0,785	0,783
p_{f_3}	0,77	0,776	0,781	0,78	0,783	0,79	0,789	0,788
$N\ [rpm]$	0	0	0	0	0	0	0	0

- f = 50 Hz

$I\ [A]$	0,2	0,4	0,6	0,8	1	1,2	1,4	1,6
$U_1\ [V]$	9,8	18,7	28,4	37,5	46,5	56	64,5	73,1
$U_2\ [V]$	9,8	18,8	28,8	37,8	46,8	57,1	65,6	73,7
$U_3\ [V]$	9	18,5	28,5	37,6	46,5	56,9	65	73
$I_1\ [A]$	0,21	0,4	0,61	0,81	1	1,21	1,4	1,6
$I_2\ [A]$	0,2	0,38	0,58	0,77	0,95	1,17	1,35	1,55
$I_3\ [A]$	0,18	0,37	0,57	0,76	0,95	1,17	1,35	1,55
$P_1\ [kW]$	0,002	0,006	0,012	0,022	0,034	0,051	0,067	0,085
$P_2\ [kW]$	0,002	0,006	0,012	0,022	0,034	0,051	0,067	0,085
$P_3\ [kW]$	0,001	0,004	0,012	0,02	0,032	0,048	0,063	0,081
$Q_1\ [kVAr]$	0,002	0,007	0,017	0,031	0,046	0,068	0,09	0,116
$Q_2\ [kVAr]$	0,002	0,007	0,017	0,029	0,044	0,067	0,088	0,114
$Q_3\ [kVAr]$	0,002	0,007	0,016	0,029	0,044	0,067	0,088	0,113
p_{f_1}	0,833	0,8	0,729	0,726	0,74	0,743	0,737	0,735
p_{f_2}	0,833	0,8	0,727	0,762	0,757	0,755	0,753	0,747
p_{f_3}	0,8	0,631	0,711	0,708	0,727	0,726	0,73	0,72
$N\ [rpm]$	0	0	0	0	0	0	0	0

- f = 60 Hz

$I\ [A]$	0,7	0,9	1	1,1	1,2	1,3	1,4	1,5
$U_1\ [V]$	*38,8*	*47,4*	*54,5*	*59,1*	*63,4*	*68,1*	*72,1*	*77*
$U_2\ [V]$	*40,4*	*48,2*	*55,3*	*59,9*	*64,1*	*68,9*	*72,8*	*77,9*
$U_3\ [V]$	*40,3*	*47,9*	*55*	*59,6*	*63,9*	*68,7*	*72,6*	*77,5*
$I_1\ [A]$	*0,77*	*0,89*	*1,02*	*1,11*	*1,2*	*1,29*	*1,37*	*1,48*
$I_2\ [A]$	*0,74*	*0,86*	*0,99*	*1,08*	*1,17*	*1,26*	*1,34*	*1,45*
$I_3\ [A]$	*0,77*	*0,9*	*1,03*	*1,12*	*1,21*	*1,3*	*1,38*	*1,49*
$P_1\ [kW]$	*18,67*	*27,51*	*36,41*	*42,97*	*49,76*	*57,54*	*64,90*	*74,64*
$P_2\ [kW]$	*19,70*	*27,98*	*37,17*	*43,93*	*50,70*	*58,77*	*65,95*	*76,24*
$P_3\ [kW]$	*20,82*	*29,57*	*38,86*	*45,93*	*52,89*	*61,27*	*68,73*	*78,52*
$Q_1\ [kVAr]$	*23,32*	*31,99*	*42,01*	*49,57*	*57,55*	*66,38*	*74,47*	*86,11*
$Q_2\ [kVAr]$	*22,49*	*30,58*	*40,19*	*47,49*	*55,27*	*63,89*	*71,89*	*83,34*
$Q_3\ [kVAr]$	*23,01*	*31,37*	*41,22*	*48,44*	*56,40*	*64,98*	*72,90*	*84,67*
p_{f_1}	*0,625*	*0,652*	*0,655*	*0,655*	*0,654*	*0,655*	*0,657*	*0,655*
p_{f_2}	*0,659*	*0,675*	*0,679*	*0,679*	*0,676*	*0,677*	*0,676*	*0,675*
p_{f_3}	*0,671*	*0,686*	*0,686*	*0,688*	*0,684*	*0,686*	*0,686*	*0,68*
$N\ [rpm]$	*0*	*0*	*0*	*0*	*0*	*0*	*0*	*0*

Annex D: Magnetization Parameters for the no load test

- f = 30 Hz

$\frac{U_{savg}}{f}$	1.558	1.863	2.168	2.43	2.715	3.003	3.552	3.8
$R_c(\Omega)$	496.16	620.41	776.80	880.84	955.82	1012.50	1011.97	1029.38
$L_m = \frac{X_m}{2\pi f}(mH)$	615	602	602	586	570	549	538	528

- f=40 Hz

$\frac{U_{savg}}{f}$	1.558	1.863	2.168	2.43	2.715	3.003	3.552	3.8
$R_c(\Omega)$	614.21	840.56	985.87	1134.16	1221.17	1288.84	1309.74	1319.16
$L_m = \frac{X_m}{2\pi f}(mH)$	620	605	593	677	571	544	537	528

- f=50 Hz

$\frac{U_{savg}}{f}$	1.558	1.863	2.168	2.43	2.715	3.003	3.552	3.8
$R_c(\Omega)$	183.08	627.03	997.12	1309.23	1536.35	1671.36	1748.04	1621.72
$L_m = \frac{X_m}{2\pi f}(mH)$	575	620	619	604	578	550	501	436

- f=60 Hz

$\frac{U_{savg}}{f}$	1.558	1.863	2.168	2.43	2.715	3.003	3.552	3.8
$R_c(\Omega)$	1007,25	1324,35	1557,96	1749,73	1886,60	1918,92	1920,86	1923,83
$L_m = \frac{X_m}{2\pi f}(mH)$	612	610	597	578	551	526	526	527

Annex E. Equations that determine the coefficients D_x, A_x and B_x

- Equations from D_5 to D_0;

$$D5 = -2b * Xm\text{^}2 * Xr\text{^}2 * \left((Rm + Rs) * Xl^2 + Rl * Xs^2\right)$$	(E.1)
$$D4 = \left(\left(Rl * Xr^2 + 2 * Rl * Xr * Xs + Rl * Xs^2 + Xl^2 * (Rr + Rs)\right) * Rm^1 + \left((Xl^2 * b^2 + Rl^2 + 2 * Rl * Rs) * Xr^2 + \left(2 * \left(Rl * Xs^2 + \left(\frac{1}{2}\right) * Xl^2 * (Rr + 2 * Rs)\right)\right) * Rr\right) * Rm + (Rl^2 * Rs + (Xs^2 * b^2 + Rs^2) * Rl + b^2 * Rs * Xl^2) * Xr^2 + Rr^2 * (Rl * Xs^2 + Rs * Xl^2)\right) * Xm^2 + 2 * Rm^2 * Xr * (Rl * Xr * Xs + Rl * Xs^2 + Rs * Xl^2) * Xm + Rm^2 * Xr^2 * (Rl * Xs^2 + Rs * Xl^2)$$	(E.2)
$$D_2 = -\left(2b * \left(\left(\left((Xr + Xs)^2 * Rl + \left(\frac{1}{2}\right) * Xl^2 * (Rr + 2 * Rs)\right) * Xm^2 + 2 * Xr * (Xs * (Xr + Xs) * Rl + Rs * Xl^2) * Xm + Xr^2 * (Rl * Xs^2 + Rs * Xl^2)\right) * Rm^2 + Xm^2 * (Rl^2 * Xr^2 + (Rr * Xs^2 + 2 * Rs * Xr^2) * Rl + Rr * Rs * Xl^2) * Rm + Rl * Rs * Xm^2 * Xr^2 * (Rl + Rs)\right)\right)$$	(E.3)
$$D_2 = \left((Rr + Rs) * Xm^2 + 2 * Rs * Xr * Xm + Rs * Xr^2\right) * Rm^2 + Xm^2 * (Xr^2 * b^2 + Rr^2 + 2 * Rr * Rs) * Rm + Rs * Xm^2 * (Xr^2 * b^2 + Rr^2)\right) * Rl^2 + \left(\left((Xr^2 * b^2 + 2 * Xr * Xs * b^2 + Xs^2 * b^2 + Rr^2 + 2 * Rr * Rs + Rs^2) * Xm^2 + \left(2 * Rs^2 * Xr + 2 * Xs * (Xr^2 * b^2 + Xr * Xs * b^2 + Rr^2)\right) * Xm + Rs^2 * Xr^2 + Xs^2 * (Xr^2 * b^2 + Rr^2)\right) * Rm^2 + 2 * Rs * Xm^2 * (Xr^2 * b^2 + Rr^2 + Rr * Rs) * Rm + Rs^2 * Xm^2 * (Xr^2 * b^2 + Rr^2)\right) * Rl + Rm^2 * Rs * Xl^2 * (Xm^2 * b^2 + 2 * Xm * Xr * b^2 + Xr^2 * b^2 + Rr^2)$$	(E.4)
$$D_1 = -Rl * Rm * b * \left(\left(2 * (Xm + Xr)^2 * Rs^2 + \left((2 * Rl + 2 * Rr) * Xm^2 + 4 * Rl * Xr * Xm + 2 * Rl * Xr^2\right) * Rs + Rl * Rr * Xm^2\right) * Rm + 2 * Rr * Rs * Xm^2 * (Rl + Rs)\right)$$	(E.5)
$$D_0 = (Rl + Rs)Rl\left((Xm + Xr)^2 b^2 + Rr^2\right)Rm^2 Rs$$	(E.6)

- Equations from A_7 to A_0;

$A_7 = 2b * {X_L}^2 * {X_m}^2 * {X_r}'^2 * {X_s}^2$	(E.7)
$A_6 = \Big(\big((Xs^2 * b^2 + (Rm + Rs)^2) * Xr^2 + 2 * Rm^2 * Xr * Xs + Xs^2 * (Rm + Rr)^2\big) * Xm^2 + 2 * Rm^2 * Xr * Xs * (Xs + Xr) * Xm + Rm^2 * Xr^2 * Xs^2\Big) * {X_L}^2 + {R_L}^2 * {X_m}^2 * {X_r}^2 * {X_s}^2$	(E.8)
$A_5 = -\Big(2b * \Big(\big(((Xs + Xr)^2 * Rm^2 + (Rr * Xs^2 + 2 * Rs * Xr^2) * Rm + Rs^2 * Xr^2) * Xm^2 + 2 * Rm^2 * Xr * Xs * (Xs + Xr) * Xm + Rm^2 * Xr^2 * Xs^2\big) * Xl^2 + Rl^2 * Xm^2 * Xr^2 * Xs^2\Big)\Big)$	(E.9)
$A_4 = \Big(\big((Xr^2 * b^2 + 2 * Xs * b^2 * Xr + Xs^2 * b^2 + (Rr + Rs)^2) * Xl^2 + Rl^2 * (Xs + Xr)^2\big) * Rm^2 + \Big(\big(2 * \big(Xr^2 * b^2 + Rr * (Rr + Rs)\big)\big) * Rs * Xl^2 + 2 * Rl^2 * (Rr * Xs^2 + Rs * Xr^2)\Big) * Rm + Rs^2 * (Xr^2 * b^2 + Rr^2) * Xl^2 + \big((Xs^2 * b^2 + Rs^2) * Xr^2 + Xs^2 * Rr^2\big) * Rl^2\Big) * Xm^2 + 2 * Rm^2 * \big((Xs * b^2 * Xr^2 + (Xs^2 * b^2 + Rs^2) * Xr + Xs * Rr^2) * Xl^2 + Rl^2 * Xr * Xs * (Xs + Xr)\big) * Xm + Rm^2 * \Big(\big((Xs^2 * b^2 + Rs^2) * Xr^2 + Xs^2 * Rr^2\big) * Xl^2 + Rl^2 * Xr^2 * Xs^2\Big)$	(E.10)
$A_3 = -\Big(2b * \Big(\big(\big(Rl^2 * (Xs + Xr)^2 + Rs * Xl^2 * (Rr + Rs)\big) * Xm^2 + 2 * Xr * (Xs * (Xs + Xr) * Rl^2 + Rs^2 * Xl^2) * Xm + Xr^2 * (Rl^2 * Xs^2 + Rs^2 * Xl^2)\big) * Rm^2 + \big((Rr * Xs^2 + 2 * Rs * Xr^2) * Rl^2 + Rr * Rs^2 * Xl^2\big) * Xm^2 * Rm + Rl^2 * Rs^2 * Xm^2 * Xr^2\Big)\Big)$	(E.11)
$A_2 = \Big(\big((Xr^2 * b^2 + 2 * Xr * Xs * b^2 + Xs^2 * b^2 + Rr^2 + 2 * Rr * Rs + Rs^2) * Xm^2 + \big(2 * Rs^2 * Xr + 2 * Xs * (Xr^2 * b^2 + Xr * Xs * b^2 + Rr^2)\big)\big) * Xm + Rs^2 * Xr^2 + Xs^2 * (Xr^2 * b^2 + Rr^2)\Big) * Rl^2 + Rs^2 * Xl^2 * (Xm^2 * b^2 + 2 * Xm * Xr * b^2 + Xr^2 * b^2 + Rr^2)\Big) * Rm^2 + 2 * Rl^2 * Rs * Xm^2 * (Xr^2 * b^2 + Rr^2 + Rr * Rs) * Rm + Rl^2 * Rs^2 * Xm^2 * (Xr^2 * b^2 + Rr^2)$	(E.12)
$A_1 = -\Big(2 * b * Rl^2 * Rm * Rs * \big(((Xm + Xr)^2 * Rs + Rr * Xm^2) * Rm + Rr * Rs * Xm^2\big)\Big)$	(E.13)
$A_0 = ((X_m + X_r)^2 * b^2 + Rr^2) * Rl^2 * Rm^2 * Rs^2$	(E.14)

- Equations from B_5 to B_0;

$B_5 = 2 * X_L * {X_m}^2 * {X_r}^2 * X_s * b * (X_s + X_L)$	(E.15)
$B_4 = \Big(\big((-Xr^2 * b^2 - Rm^2 - 2 * Rm * Rr - Rr^2) * Xs - Rm^2 * Xr\big) * Xm^2 - Rm^2 * Xr * (Xr + 2 * Xs) * Xm - Rm^2 * Xr^2 * Xs\Big) * Xl^2 + \Big(\big((-Xr^2 * b^2 - Rm^2 - 2 * Rm * Rr - Rr^2) * Xs^2 - 2 * Rm^2 * Xr * Xs - Xr^2 * (Rm + Rs)^2\big) * Xm^2 - 2 * Rm^2 * Xr * Xs * (Xs + Xr) * Xm - Rm^2 * Xr^2 * Xs^2\Big) * Xl - Rl^2 * Xm^2 * Xr^2 * Xs$	(E.16)
$B_3 = \Big(2b * \Big(Rm * \Big((Xm + Xr) * \big((Xs + Xr) * Xm + Xs * Xr\big) * Rm + Rr * Xm^2 * Xs\Big) * Xl^2 + \Big(\big((Xs + Xr) * Xm + Xs * Xr\big)^2 * Rm^2 + Xm^2 * (Rr * Xs^2 + 2 * Rs * Xr^2) * Rm + Rs^2 * Xm^2 * Xr^2\Big) * Xl + Rl^2 * Xm^2 * Xr^2 * Xs\Big)\Big)$	(E.17)
$B_2 = \Big(\big(-b^2 * (Xs + Xr) * Xl^2 + (-Xr^2 * b^2 - 2 * Xs * b^2 * Xr - Xs^2 * b^2 - (Rr + Rs)^2) * Xl - Rl^2 * (Xs + Xr)\big) * Xm^2 + \big(-Xr^2 * b^2 - 2 * Xr * Xs * b^2 - Rr^2\big) * Xl^2 + \big(-2 * Xs * b^2 * Xr^2 + (-2 * Xs^2 * b^2 - 2 * Rs^2) * Xr - 2 * Xs * Rr^2\big) * Xl - Rl^2 * Xr * (Xr + 2 * Xs)\Big) * Xm - Xs * (Xr^2 * b^2 + Rr^2) * Xl^2 + \Big(\big(-Xs^2 * b^2 - Rs^2\big) * Xr^2 - Xs^2 * Rr^2\Big) * Xl - Rl^2 * Xr^2 * Xs\Big) * Rm^2 - \Big(2 * \Big(\big(Xr^2 * b^2 + Rr * (Rr + Rs)\big) * Rs * Xl + Rl^2 * Rr * Xs\Big)\Big) * Xm^2 * Rm - Xm^2 * (Xr^2 * b^2 + Rr^2) * (Rl^2 * Xs + Rs^2 * Xl)$	(E.18)
$B_1 = 2 * b * Rm * \Big(\big((Rl^2 * (Xs + Xr) + Rs * (Rr + Rs) * Xl) * Xm^2 + Xr * \big((Xr + 2 * Xs) * Rl^2 + 2 * Rs^2 * Xl\big) * Xm + Xr^2 * (Rl^2 * Xs + Rs^2 * Xl)\big) * Rm + Rr * Xm^2 * (Rl^2 * Xs + Rs^2 * Xl)\Big)$	(E.19)
$B_0 = -Rm^2 * \Big(\big(\big((Xs + Xr) * Xm + Xs * Xr\big) * Rl^2 + Rs^2 * Xl * (Xm + Xr)\big) * (Xm + Xr) * b^2 + Rr^2 * \big((Xm + Xs) * Rl^2 + Rs^2 * Xl\big)\Big)$	(E.20)

Annex F. Experimental results for different resistances

R = 411 Ω

			Voltage (V)			Current (A)			Power (kW)			Power Factor		
$N\ (rpm)$		$C(\mu F)$	U_1	U_2	U_3	I_1	I_2	I_3	P_1	P_2	P_3	pf_1	pf_2	pf_3
432	476	160	70.8	69.8	71.2	1.58	1.50	1.50	0.010	0.013	0.008	0.092	0.120	0.079
432	500	135	77	76.2	77.8	1.62	1.59	1.51	0.013	0.013	0.019	0.101	0.142	0.085
496	582	90	100.8	100.9	100	1.64	1.62	1.63	0.019	0.022	0.019	0.117	0.127	0.115
562	620	80	107	107.1	105.8	1.55	1.54	1.55	0.022	0.024	0.022	0.130	0.143	0.131
595	675	65	153.3	155.6	151.0	1.60	1.60	1.61	0.042	0.047	0.047	0.173	0.189	0.193
713	762	50	134.5	134.2	137.7	1.65	1.65	1.65	0.035	0.044	0.041	0.092	0.120	0.090
734	816	45	149.5	150.6	148.8	1.61	1.58	1.62	0.045	0.048	0.046	0.184	0.199	0.191
786	875	35	159.1	159.6	157.1	1.57	1.56	1.57	0.050	0.056	0.052	0.200	0.224	0.212
855	939	30	175.5	176.7	174.2	1.69	1.64	1.71	0.062	0.088	0.066	0.210	0.232	0.222
950	1016	25	185.9	185.3	181.8	1.55	1.55	1.55	0.069	0.079	0.074	0.241	0.273	0.336
1192	1276	20	227.6	229.6	224.5	1.53	1.52	1.54	0.109	0.117	0.115	0.316	0.334	0.336

R = 206 Ω

			Voltage (V)			Current (A)			Power (kW)			Power Factor		
N (rpm)		C(μF)	U_1	U_2	U_3	I_1	I_2	I_3	P_1	P_2	P_3	pf_1	pf_2	pf_3
558	601	100	87.0	87.6	86.8	1.59	1.58	1.60	0.034	0.034	0.023	0.244	0.245	0.232
644	689	75	103.5	104.7	103.3	1.58	1.57	1.60	0.048	0.049	0.047	0.294	0.298	0.285
681	694	75	103.3	103.9	103.3	1.57	1.57	1.60	0.047	0.047	0.046	0.294	0.297	0.284
681	743	65	112.8	114.1	112.9	1.63	1.62	1.64	0.058	0.058	0.056	0.314	0.314	0.305
718	771	45	115.2	116.3	114.8	1.57	1.55	1.58	0.047	0.047	0.046	0.294	0.297	0.284
851	881	50	133.0	135.0	133.5	1.58	1.55	1.60	0.082	0.082	0.081	.384	0.392	0.278
987	1020	35	151.3	153.8	152.8	1.64	1.61	1.66	0.106	0.109	0.108	0.432	0.441	0.426
1076	1146	30	159.5	161.7	159.0	1.58	1.57	1.58	0.119	0.120	0.117	0.478	0.469	0.464